THE
EMBO
JOURNAL

TRANSPARENT
PROCESS

ER arrival sites for COPI vesicles localize to hotspots of membrane trafficking

Saskia Schröter, Sabrina Beckmann & Hans Dieter Schmitt[*]

Abstract

COPI-coated vesicles mediate retrograde membrane traffic from the *cis*-Golgi to the endoplasmic reticulum (ER) in all eukaryotic cells. However, it is still unknown whether COPI vesicles fuse everywhere or at specific sites with the ER membrane. Taking advantage of the circumstance that the vesicles still carry their coat when they arrive at the ER, we have visualized active ER arrival sites (ERAS) by monitoring contact between COPI coat components and the ER-resident Dsl tethering complex using bimolecular fluorescence complementation (BiFC). ERAS form punctate structures near Golgi compartments, clearly distinct from ER exit sites. Furthermore, ERAS are highly polarized in an actin and myosin V-dependent manner and are localized near hotspots of plasma membrane expansion. Genetic experiments suggest that the COPI•Dsl BiFC complexes recapitulate the physiological interaction between COPI and the Dsl complex and that COPI vesicles are mistargeted in *dsl1* mutants. We conclude that the Dsl complex functions in confining COPI vesicle fusion sites.

Introduction

The secretory pathway is a multi-step process with the endoplasmic reticulum (ER) as the starting point, the Golgi apparatus as a sorting hub and lysosome or plasma membrane as two main destinations. Vesicles and tubules are the main carriers that mediate transport between these organelles. The concomitant loss of material from the membrane compartments has to be compensated either by *de novo* synthesis and fresh supply of material, or by retrograde transport (Pelham, 1996). Since retrograde transport also involves the re-routing of material via additional organelles like the early and recycling endosomes, the cells are crowded with a large number of carriers with different origins and destinations. Thus, the arrival and exit of material at a particular organelle has to be carefully organized.

One way to manage the simultaneous arrival and departure of material is the spatial separation of exit and entry sites within one organelle. Remarkably, the initial and the final steps of secretory pathway are best characterized in respect to such a spatial organization. At the endoplasmic reticulum, COPII vesicles always form within defined regions called ER exit sites (ERES), also termed transitional ER (Bannykh *et al*, 1996). In highly polarized cells like yeast cells (*Saccharomyces cerevisiae*) or nerve cells, the secretory vesicles fuse at the plasma membrane within areas marked by the polarisome (Pruyne *et al*, 1998; Sheu *et al*, 1998; McCusker *et al*, 2012) or the scaffold of the presynaptic active zone in nerve cells, respectively (Jahn & Fasshauer, 2012; Chua, 2014). At the rim of these exocytic regions, one finds areas of active internalization (McCusker *et al*, 2012). Clearly, the actin cytoskeleton plays an important role in the arrangement of spots of highest exocytic and endocytic activities in yeast and nerve terminals (Li & Gundersen, 2008; Nelson *et al*, 2013). Marker proteins for exit sites can be scaffolding factors, proteins required for the vesicle formation, or coat proteins themselves. In case of the ERES, the scaffolding protein Sec16p or the COPII coat subunit Sec24p are often used in yeast and mammalian cells (Shaywitz *et al*, 1997; Shindiapina & Barlowe, 2010; Bharucha *et al*, 2013). Likewise, suitable markers for the site of active clathrin-mediated endocytosis are the clathrin coat complex itself or dynamin 2, a protein involved in vesicle formation (Rappoport & Simon, 2003). Similarly, the site of vesicle fusion at the plasma membrane in yeast can be identified by staining proteins present on secretory vesicles like the small GTPase Sec4p or proteins that reside at the plasma membrane like Sec3p, a subunit of the exocyst tethering complex present at the plasma membrane (Finger *et al*, 1998).

For Golgi membranes and endosomes, the sites of vesicle formation and fusion seem to be less clearly segregated. At the Golgi, the formation of COPI-coated vesicles seems to be restricted to the edges of cisternae (Ladinsky *et al*, 1999; Klumperman, 2011). On the surface of endosomes, a separation of large domains of similar size has been observed based on the presence of different GTPases of the Rab/Ypt superfamily, as well as different phosphoinositides (Miaczynska & Zerial, 2002; Jean & Kiger, 2012). In contrast to the well-characterized ERES, however, we know next to nothing about the sites where the incoming COPI vesicles fuse with the ER in *Saccharomyces cerevisiae* or mammalian cells. In fact, to date it has been impossible to visualize postulated ER arrival sites (ERAS)

Department of Neurobiology, Max Planck Institute for Biophysical Chemistry, Göttingen, Germany
  *Corresponding author. Tel: +49 551 201 1652; E-mail: hschmit@mpibpc.mpg.de

(Spang, 2009, 2012). The alternative term "ER import sites" (ERIS) was later introduced by plant researchers (Lerich *et al*, 2012). The situation is different in the yeast *Pichia pastoris* and in plant cells, where COPI and COPII vesicles are confined to a narrow interface between closely apposed ER and the stacked Golgi membranes (Rossanese *et al*, 1999; Lerich *et al*, 2012). In these cells, closely confined ER arrival sites may be the result of a tight apposition of Golgi and ER membranes. To identify ER arrival sites in budding yeast or mammalian cells, tethering complexes may be suitable marker proteins. They are thought to make the first contact between incoming vesicles and the target membrane. Many of them interact with SNARE proteins, the actual catalysts of membrane fusion (Yu & Hughson, 2010). This is also true for the Dsl complex in yeast. This complex is responsible for the tethering of Golgi-derived COPI vesicles to the ER. One of its three subunits, Dsl1p, carries a lasso domain, which can bind two of the seven COPI subunits, α-COP and δ-COP *in vitro* (Andag & Schmitt, 2003; Ren *et al*, 2009; Zink *et al*, 2009). The other two Dsl subunits, Dsl3(Sec39)p and Tip20p, are in a tight complex with the SNAREs Use1p and Sec20p at the ER (Kraynack *et al*, 2005; Ren *et al*, 2009). In mammalian cells, the equivalent of the Dsl complex, the NRZ complex, also interacts with COPI vesicles. It additionally requires the UVRAG protein for this interaction (Hirose *et al*, 2004; He *et al*, 2013).

In contrast to the aforementioned exocyst, the Dsl complex and its associated SNAREs are distributed uniformly over the ER (Kraynack *et al*, 2005; Meiringer *et al*, 2011). This may indicate that COPI vesicles fuse uniformly across the ER. Contrasting evidence came from our previous work, showing that COPI vesicles accumulate next to COPII-positive ER domains upon Dsl1p depletion (Zink *et al*, 2009), suggesting an association of ER arrival sites with ER exit sites. Thus, the conventional approach of visualizing possible ER arrival sites through a single marker protein did not yield conclusive evidence for or against the existence of specifically confined ER arrival sites. We therefore set out to map ER arrival sites in living yeast, using a more elaborate approach. Two previous findings were crucial for that: (i) COPI vesicles that arrive at the ER still carry their coat (Zink *et al*, 2009) and (ii) the Dsl complex contains several COPI binding sites (Andag & Schmitt, 2003; Zink *et al*, 2009; Diefenbacher *et al*, 2011; Suckling *et al*, 2015). A recent study by Dodonova *et al* (2015), which presents the full structure of the COPI coat, has confirmed that the Dsl1p binding sites of COPI subunits are well accessible at the surface of the COPI coat, thereby corroborating the plausibility of an interaction. We made use of these findings by employing bimolecular fluorescence complementation (BiFC) as a probe to visualize sites of interaction between COPI coat and Dsl complex at the ER. This "split-GFP technique" relies on the formation of a fluorescent reporter protein by association of its N-terminal and C-terminal fragments, provided that the proteins carrying these fragments as tags come into close proximity. One caveat of this approach is that, under several *in vitro* conditions, the formation of bimolecular fluorescent complexes was found to be irreversible (Ghosh *et al*, 2000; Hu *et al*, 2002; Magliery & Regan, 2005). Magliery *et al* (2005) suggested, however, that this property would make the BiFC approach suitable for the visualization of otherwise transient interactions. This strategy was successfully applied by Morell *et al* (2007). Moreover, BiFC-mediated fluorescence signals have been reported to change dynamically *in vivo* in response to cell stimuli and associated protein–protein interaction

states (Schmidt *et al*, 2003; Guo *et al*, 2005). This technique has also been used in yeast for the analysis of proteins interactions in membrane traffic (Lipatova *et al*, 2012; Mao *et al*, 2013; Weber-Boyvat *et al*, 2013). Since interactions between Dsl1p and COPI coat are very weak or transient (Zink *et al*, 2009), the BiFC technique appeared suitable for identifying the sites where they interact in the cells.

We introduced segments encoding parts of the YFP variant Venus (vYFP) (Sung & Huh, 2007) at the chromosomal loci of genes whose products are involved in transport between ER and Golgi. This included four COPI subunits, the two Dsl subunits Dsl1p and Dsl3p, a cargo receptor, and proteins involved in COPII vesicle formation. Because of the potential irreversibility of YFP fragment complementation, we performed meticulous controls to ensure continued functionality of the involved transport processes. By analyzing the growth characteristics of a large number of BiFC combinations in mutant background, we found evidence for a quite efficient reconstitution of the normal COPI•Dsl interaction by the BiFC complexes. Taken together, our data suggest that the BiFC spots in fact represent specific domains where Golgi-derived vesicles fuse with the ER. We confirm the notion that COPI vesicles are at least partially coated upon their arrival at the ER.

The emerging picture indicates that COPI vesicles do not fuse randomly across the ER. Rather, ERAS are highly ordered and are localized in a polarized manner, thereby showing a different pattern from ER exit sites. With these new insights, we help build a more detailed picture of intracellular transport routes.

Results

Construction and validation of BiFC strains

We performed bimolecular fluorescence complementation (BiFC) assays to assess whether COPI-coated vesicles or membranes establish contact with the ER in yeast. The system we employed utilizes the N- and C-terminal fragments (VN and VC) of vYFP (Venus version of the yellow fluorescent protein; Nagai *et al*, 2002; Sung & Huh, 2007). They comprise residues 1–172 (VN) or 155–238 (VC) of the fluorescent protein, respectively, and were introduced at the chromosomal loci of the corresponding genes. Figure 1A lists the genes analyzed here and provides information about the kind of modification that was introduced at each site as well as a graphic representation of all examined BiFC connections. Most single- and double-tagged (expressing a VN- and a VC-tagged protein) strains were fully viable even at 37°C (Figs EV1H and EV2, and Appendix Fig S1). We confirmed the expression of the BiFC-tagged proteins through immunoblots (Fig EV1B–G). Compared to wild-type protein levels, levels of tagged proteins were either reduced or equal to wild type. Importantly, the formation of BiFC complexes in cells expressing VN as well as VC-tagged genes did not affect the expression levels (Fig EV1D–G). Most of the localization experiments involving a COPI subunit were performed using either β'-COP or ε-COP (β'-COP^{VN} or ε-COP^{VC}), two COPI subunits that exhibited either normal or reduced expression levels as determined by Western blotting. To analyze whether the introduction of BiFC tags affects retrograde transport routes, we checked the protein levels of the Golgi proteins Emp47p and Rer1p in BiFC strains. Both proteins cycle

Figure 1. Specificity of BiFC signals and effects of BiFC formation on cell viability.

A   Schematic representation of all BiFC combinations studied in this work (lime green cartoons: the two most commonly used BiFC pairs β'-COP^{VN}•Dsl3p^{VC} and Dsl1p^{VN}•ε-COP^{VC}; dashed lines: all other BiFC pairs presented in this work). All BiFC-tagged proteins are listed in the table.

B   Bimolecular fluorescence complementation between subunits of the Dsl complex and the COPI coat. The BiFC pair β'-COP^{VN}•Dsl3p^{VC} yielded fluorescent foci that showed dramatically reduced fluorescence intensity in the COPI binding-deficient *dsl1-5xWA* mutant. Schematic yeast cell representations depict the typical BiFC foci localization patterns. Scale bar, 10 μm.

C   Quantification of the β'-COP^{VN}•Dsl3p^{VC} BiFC signals in wild-type cells and in COPI binding-deficient *dsl1-5xWA* and *dsl1-Δlasso* mutants (as shown exemplarily in B). Mean values + SEM of at least three independent experiments (*n* = 3–8) are displayed. Statistical analysis was carried out by comparing the number of cells with BiFC signals over integrated thresholds to those without signals (*P < 0.05). *dsl1* mutant strains show a significant decrease in brightness, spot number, and spot size in comparison with their corresponding *DSL1* wild-type strains (two-sample t-test). The *dsl1-5xWA* mutation also led to comparable signal reduction in cells carrying the VN^{I152L} variant in the β'-COP$^{VN\ I152L}$•Dsl3p^{VC} combination. ***P < 0.001.

D   Subcellular localization of different BiFC-tagged protein pairs. The Dsl1p^{VN}•Dsl3p^{VC} combination involving subunits of the ER-resident Dsl1 complex exhibited typical ER localization. Sec16p^{VN}•Sec16p^{VC} signals in a diploid heterozygous strain displayed a pattern typical for ER exit sites, while diploid cells carrying the α-COP^{VN}•α-COP^{VC} BiFC pair showed a Golgi-like fluorescence pattern. Scale bar, 10 μm.

E   The localization of COPI•Dsl BiFC foci compared to the autophagy marker Ape1p. Double fluorescence micrographs of the BiFC pair β'-COP^{VN}•Dsl3p^{VC} and the autophagy marker ^{mRFP}Ape1p are superimposed with the DIC image. BiFC-YFP signals are pseudocolored green. Fluorescent signals appeared distinct from each other. Also no co-localization was observed when we analyzed COPI•COPII(Sec16p) BiFC spots in cells expressing mRFP tagged *APE1* (S. Beckmann, unpublished results). Scale bar, 10 μm.

F   Growth effects of Venus fragment tags in *dsl1* mutant cells. Serial tenfold dilutions of liquid cell cultures were spotted on agar plates and incubated at 30°C for 2 days. The images in the second row show that β'-COP^{VN}-producing cells expressing the *dsl1-5xWA* mutation could not grow. The complementation of β'-COP^{VN} by its cognate interaction partners Dsl1p^{VC} and Dsl3p^{VC}, but not by non-cognate BiFC partners (Sec24p^{VC}, Sec16p^{VC}, or ^{VC}Rer1p), suppressed these growth defects. Spot assays of exemplary BiFC partners are depicted. Asterisk: Dsl1p^{VC} carrying the *dsl1-5xWA* defect was expressed from a plasmid. See Figs EV1 and EV2 and Appendix Fig S1 for full data display.

G   BiFC signal quantifications of the strains presented in (F). β'-COP^{VN} yielded BiFC fluorescence signals with all tested complementation partners. This rules out the possibility that the lack of suppression observed in (F) simply reflects the inability of the BiFC partners to form a complex and shows that the successful complementation of the split-YFP fragments does not *per se* suppress the synthetic lethal effect of the VN tag in *dsl1-5xWA* cells. Mean values + SEM of at least three independent experiments (*n* = 3–8) are displayed.

H   BiFC signal intensities greatly depend on which BiFC combination is analyzed. Fluorescence intensities of COPI•Dsl BiFC pairs (left) were much higher than those of COPII•Dsl BiFC pairs (right). Mean values + SEM of at least three independent experiments (*n* = 3–5) are displayed.

I   Localization of Dsl1p^{CFP} in β'-COP^{VN}•Dsl3p^{VC} cells. An overall ER localization of Dsl1p^{CFP} was retained in β'-COP^{VN}•Dsl3p^{VC} cells, while some of the signal was found in the foci. BiFC-YFP signals are pseudocolored red. Scale bar, 10 μm.

between Golgi and ER and require normal Golgi ER transport for their stability (Schröder-Köhne *et al*, 1998; Sato *et al*, 2001). Emp47p abundance in COPI•Dsl combinations was reduced to about 60% of the wild-type level, while the Rer1p levels were unaffected. However, the VN tag at a COPI subunit alone was sufficient to induce this reduction (Fig EV1J), suggesting that the reduction in Emp47p levels was due to the tag and not due to the formation of BiFC complexes. HDEL signal-mediated ER retrieval was intact, as the fluorescence of HDEL-tagged RFP yielded normal ER staining (Figs 4A and EV4A).

Interactions between COPI coat and Dsl complex lead to specific BiFC signals

All COPI•Dsl BiFC combinations yielded fluorescent signals with a consistent punctate subcellular distribution pattern. Figure 1B shows images of a representative BiFC pair (β'-COP^{VN}•Dsl3p^{VC}). We confirmed the specificity of the formed fluorescence signal by examining the signal intensity in either wild-type or *dsl1* mutant cells. For this, we used mutations in the lasso domain of Dsl1p, which have been shown to reduce Dsl1p binding to δ-COP and α-COP *in vitro*. We used two mutant versions: (i) *dsl1-5xWA* harboring five Trp to Ala substitutions in the lasso domain (Zink *et al*, 2009) and (ii) a mutant lacking the whole lasso domain (*dsl1-Δlasso*; this work). In both mutants, we observed a similar decrease in fluorescence signal intensity, as confirmed by the quantification of the spot number and the area covered by spots (Fig 1C). We confirmed that this effect is not due to a lower stability of the different mutant proteins (Fig EV1A). As an additional control, we replaced the VN$^{1–173}$ tag at β'-COP with a shorter mutant version (VN$^{1–155}$) that carries an Ile to Leu substitution at position 153. This has been

shown to increase the signal to noise ratio as well as reduce the probability of incorrect subcellular localization (Kodama & Hu, 2010). This modification reduced the BiFC signal equally in both wild-type and *dsl1-5xWA* mutant cells (Fig 1C). Residual binding observed in case of the mutants may be due to additional interaction sites of the COPI coat with the Dsl complex, for example, via Tip20p (Diefenbacher *et al*, 2011). We also introduced a mutation into the VC tag that prevents the self-association of YFP (Zacharias *et al*, 2002). Again, this did not affect the formation of β'-COP^{VN}•Dsl3p^{VC} spots or their specific localization (see below). Furthermore, diploid strains expressing one untagged and one VC-tagged copy of the Dsl3 proteins showed reduced intensity of the BiFC signals, but without affecting the specific localization (Fig EV1K). Finally, while some of the Dsl1p^{CFP} accumulated in BiFC punctae, the ER localization of Dsl1p^{CFP} was retained in β'-COP^{VN}•Dsl3p^{VC} cells (Fig 1I). All these lines of evidence strongly point against the notion that the BiFC spots are induced by trapping the Dsl proteins in the BiFC complexes.

The notion that BiFC signals reflect specific interactions is further substantiated by the following observations: (i) Fluorescence signals between *cis*-BiFC pairs (two subunits of one protein complex, specifically Dsl1p^{VN}•Dsl3p^{VC}, Sec16p^{VN}•Sec16p^{VC}, α-COP^{VN}•α-COP^{VC}) showed the expected subcellular localizations of the respective complexes (Fig 1D). (ii) While all *trans*-BiFC pairs (involving proteins from different complexes) probing COPI subunit interactions with either Dsl or COPII subunits gave rise to BiFC signals of similar intensity and localization, Dsl•COPII combinations showed extremely weak BiFC signals (Dsl3p^{VN}•Sec16p^{VC}, Sec16p^{VN}•Dsl3p^{VC}, or Dsl3p^{VN}•Sec24p^{VC}; Fig 1H). Therefore, these combinations may be considered additional negative controls for the BiFC combinations involving COPI subunits. (iii) The observed fluorescent foci are not degradation related since the β'-COP^{VN}•Dsl3p^{VC} BiFC spots
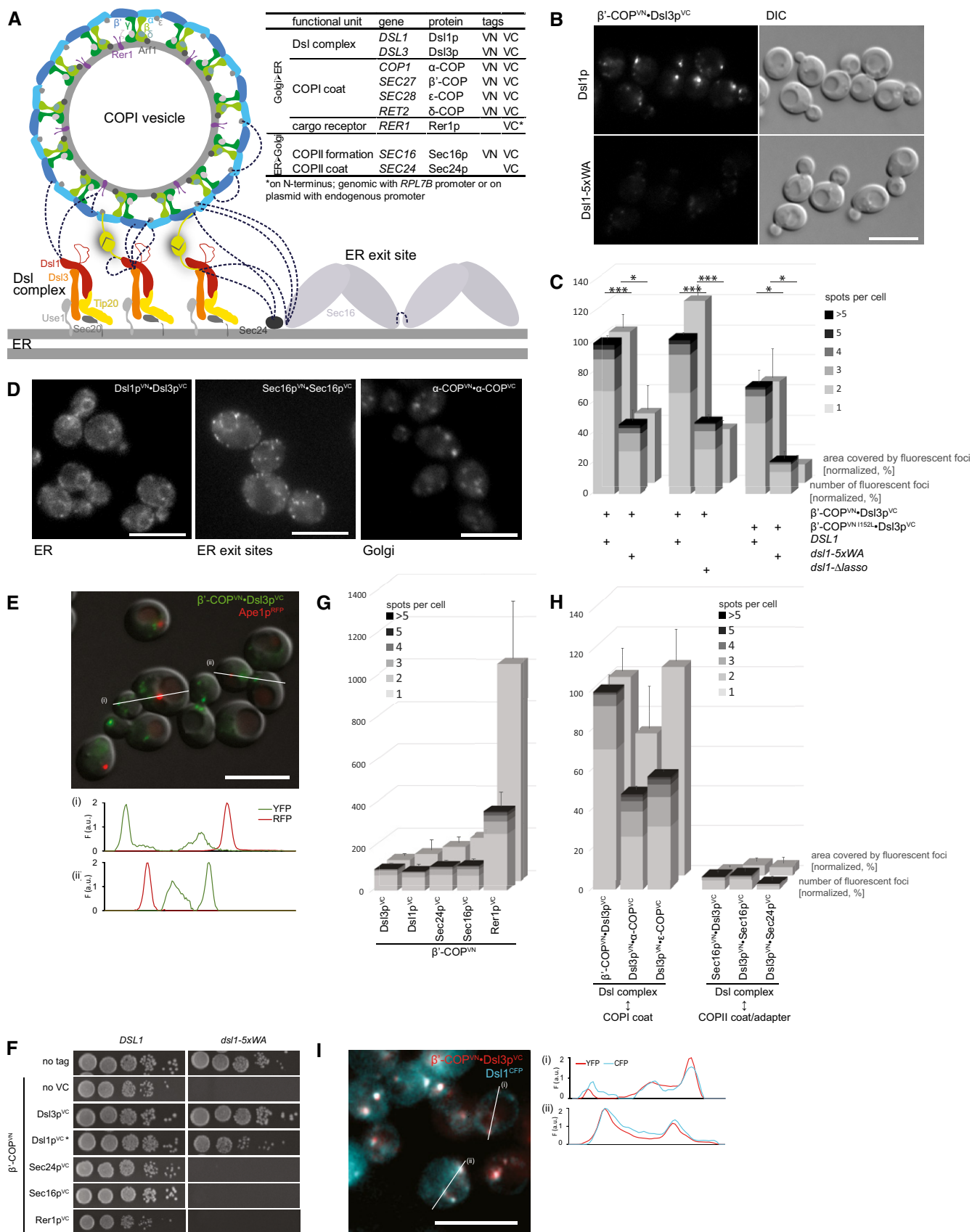
Figure 1.

did not co-localize with an autophagy marker (Fig 1E); neither did they change in number or size when autophagy was blocked by the deletion of the *ATG1* gene (H.D. Schmitt, unpublished results; Thumm *et al*, 1994). Finally, we showed that the BiFC interaction does not disturb the Dsl•SNARE interaction (Fig EV1I). The results obtained by using the ER exit site markers also confirmed our previous observation that COPI subunits come close to Dsl subunits as well as COPII subunits (Zink *et al*, 2009).

Additional evidence for the specificity of the COPI•Dsl interaction came from a series of growth assays involving *dsl1* mutants (Fig EV2, Appendix Fig S1). The reason for addressing this in a systematic way was the observation that some combinations of BiFC tags and the *dsl1-5xWA* mutation could not be obtained by crosses and tetrad analysis. We created 37 different strains that were especially designed to avoid variations caused by differences in the genetic background of mutant and wild-type cells. The growth assays were performed not only with the *dsl1-5xWA* mutation, but also with the *dsl1-22* mutation, a mutation which affects the well-conserved C-terminal E-domain (Andag *et al*, 2001; Tripathi *et al*, 2009; Schmitt, 2010). For simplicity, a representative set of results obtained with β'-COP^VN is given in Fig 1F. The growth assays confirmed the observation we had made by tetrad analysis, that is, that the *dsl1* mutations are lethal in the presence of the VN tag fused to the C-terminus of COPI subunits, α-, β'-, ε-, or δ-COP. Other tags fused to COPI subunits had varying effects. Like VN, the tetramer-forming RFP (Redstar) was lethal with *dsl1-5xWA* (Fig EV2L). GFP, which forms a weak dimer, had minor effects, while the monomeric form of RFP did not interfere with growth in the presence of *dsl1-5xWA* (Fig EV2L). Thus, it appears that the severity of the growth defect correlates with the tendency of the tag to aggregate.

Importantly, however, *dsl1* mutants are viable in the presence of the β'-COP^VN•Dsl3p^VC pair (Fig 1B and F). This suggests that the VC fragment at Dsl3p can suppress the lethality of the COPI^VN/*dsl1*

combinations. Dsl3p^VC is in fact able to suppress growth defects in all other COPI^VN/*dsl1-5xWA* combinations (α-, ε-, and δ-COP) as well, and equivalent results were obtained with the *dsl1-22* mutation (Figs 1F and EV2E–G and K). Most importantly, no suppression was observed when complementation was attempted with other ER proteins carrying the VC fragment, such as Sec16p, Sec24p, the cargo receptor Rer1p, or other COPI subunits (Figs 1F and EV2H–J). The failure of these VC-constructs to rescue cells carrying the β'-COP^VN/*dsl1-5xWA* combination was not due to an inability to form BiFC complexes (Fig 1G). Quantification of BiFC signals suggests that the tested proteins come very close to β'-COP^VN, but only the Dsl proteins seem to fulfill the requirements for a correct tethering of the COPI vesicles to suppress the growth defects. This indicates that the BiFC interaction between the COPI and Dsl complex constitutes an important function and may, therefore, resemble the normal coat–tether interaction.

Dsl1•COPI interaction sites are polarized and localize to sites of high material turnover

All examined COPI•Dsl BiFC strains listed in Fig 1A exhibited signals which were localized to the cell poles (Figs 2A and 3A–D; Movies EV1, EV2, EV3 and EV4). Moreover, the localization of the BiFC spots remained polarized when we introduced a mutation into the VC tag of Dsl3p that prevents the formation of dimers (equivalent to the A206K mutation; Zacharias *et al*, 2002; Fig 3D). Thus, the polarized localization is not due to the dimerization of the complemented YFP. In order to observe the fate of individual cells more closely, we employed time-lapse imaging to evaluate the dynamic changes of the fluorescent foci patterns. We observed that COPI•Dsl signals were localized in a polarized manner to sites of intense membrane expansion (Figs 2A and 3J; Field & Schekman, 1980; Finger *et al*, 1998): Cells entering the budding process already

Figure 2. Localization patterns of COPI•Dsl BiFC foci during growth and starvation.

A   Dsl1p^VN•ε-COP^VC BiFC signal localization pattern throughout the budding cycle. Time-lapse images of agarose-embedded cells were recorded at RT with continuous PM Glc + ura medium supply. Arrowheads mark positions of BiFC foci. Fluorescence signals exhibited a characteristic and reproducible localization pattern, which favored sites of high material turnover during budding. Scale bar, 10 μm.

B   Dsl1p^VN•ε-COP^VC BiFC foci showed different subcellular distribution depending on the growth status of cells. Cells were cultured in PM + ura medium with or without 2% glucose at 30°C for 90 min and imaged. BiFC signals dispersed under glucose starvation, resulting in an ER exit site-like fluorescence pattern. Scale bar, 10 μm.

C   The effect of carbon source depletion on COPI•Dsl BiFC signal polarization. Cells carrying Dsl1p^VN•ε-COP^VC were starved in glucose-free PM + ura medium for 90 min. Then, the medium was replaced by PM Glc + ura with 2% glucose, while imaging the cells continuously at 1-min intervals. Two exemplary cells are shown (upper and lower panel). Starvation-induced dispersed BiFC signals reversibly returned to polarized distribution within minutes after addition of glucose-containing medium. Arrowheads mark the point of signal repolarization, and arrows indicate resumed bud outgrowth. Scale bar, 5 μm.

D   β'-COP^VN•Dsl3p^VC BiFC signals during mating. Fluorescence micrographs of the BiFC pair β'-COP^VN•Dsl3p^VC (green) are superimposed with the DIC image (gray). Two haploid strains carrying β'-COP^VN•Dsl3p^VC were allowed to mate in YEPD liquid culture for 2 h at 30°C. Then, time-lapse recordings were made in agarose embedding at RT with continuous PM Glc + ura medium supply. Fluorescence signals exhibited a characteristic and reproducible localization at sites of high material turnover during zygote formation. Scale bar, 10 μm.

E   Comparison of the BiFC localization pattern in COPI•Dsl and COPI•COPI strains. Time-lapse images of agarose-embedded cells carrying the COPI•Dsl BiFC pair β'-COP^VN•Dsl3p^VC or the COPI•COPI BiFC pair β'-COP^VN•α-COP^VC were recorded at RT with continuous PM Glc + ura medium supply at 5-min intervals. Single-cell pseudokymographs were generated by concatenating the central section of the cell (sliced along the pole axis, frames at double the width of the bud neck) of a time-lapse dataset. The COPI•Dsl strain showed one single dominant spot at the bud tip and later the bud neck. In contrast, the COPI•COPI strain additionally exhibited multiple spots with no apparent polarization tendency, which were localized mainly in the mother cell. Schematic yeast cell representations depict the typical BiFC foci localization pattern of the strains. Scale bar, 10 μm.

F   Fluorescence recovery after photobleaching of BiFC signals. Time-lapse images of agarose-embedded cells carrying the β'-COP^VN•Dsl3p^VC BiFC pair were recorded at RT with PM Glc + ura medium supply at 2-min intervals. Fluorescence of ROIs marked in dashed lines (where the full cell, full bud, or only the bud foci were bleached) was depleted by three repetitions of fluorescence excitation at 177 μs/pixel and 100% laser intensity. Arrowheads: reappearing fluorescence signal; scale bar, 2 μm.

G   Densitometric measurements of fluorescence intensities in photobleached cells. Representative datasets from five independent experiments are displayed, featuring cells that had been bleached entirely (black lines), at the bud only (dark blue lines), or at the fluorescent foci at the bud tip only (light blue line). Values are displayed in percentage of initial fluorescence and were corrected for photobleaching effects by normalization against fluorescence of unbleached cells. Fluorescence recovery was typically not continued to full recovery stage because of the photobleaching artifacts occurring during long-term imaging of the samples.
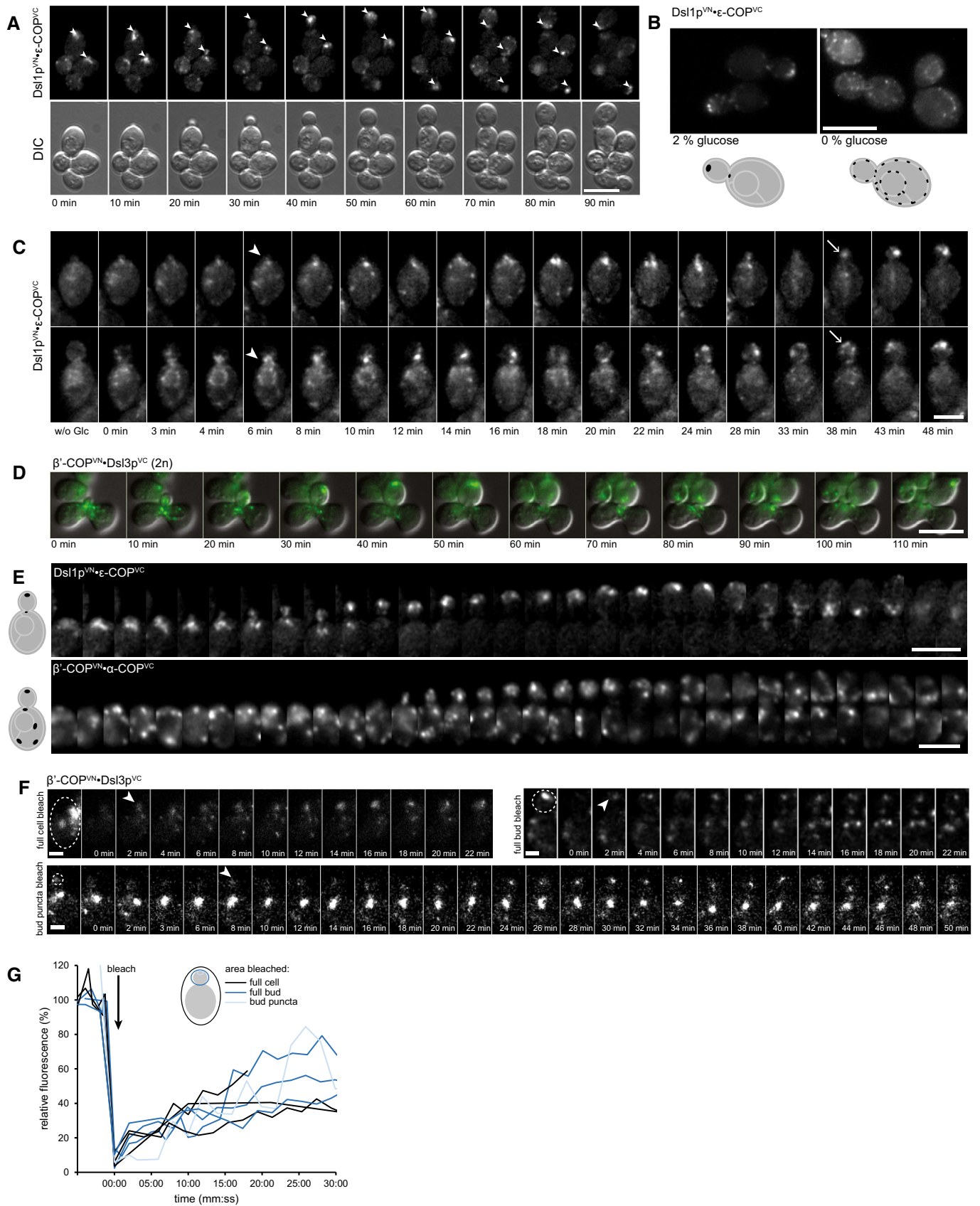
Figure 2.

▶

Figure 3. Polarization patterns of BiFC between the Dsl complex, the COPI coat, and COPI cargo.

Time-lapse micrographs of agarose-embedded cells were taken at RT with fresh PM Glc + ura medium supply throughout one budding cycle. Representative images of characteristically reoccurring fluorescence localization stages are displayed. In all combinations, fluorescence foci localized to areas of membrane outgrowth in the bud. Often, another prominent fluorescent spot was found in the mother cell on the side of the bud neck. Scale bar, 5 μm. Kymographs of all time-lapse datasets shown in this figure are presented in Fig EV3A.

A–D   Cells expressing complementary BiFC-tagged proteins between subunits of the Dsl complex and COPI were analyzed. Panel (D) shows a BiFC combination that includes a mutated VC tag. This mutation in the VC part is equivalent to the A206K mutation in GFP, which prevents the formation of YFP dimers (Zacharias *et al*, 2002).

E, F   The VC-tagged COPI vesicle cargo protein Rer1p was examined in combination with the VN-tagged COPI subunit β'-COP or the VN-tagged Dsl1 protein.

G   BiFC spots in COPI•COPII BiFC combination (β'-COP^{VN}•Sec16p^{VC}) were also polarized.

H   COPI•COPI (α-COP^{VN}•α-COP^{VC}) BiFC signals showed one spot that localized to the bud tip and, at later budding stages, to the bud neck (compare with A–G). Additionally, multiple spots with no apparent polarization tendency were observed, which are reminiscent of a Golgi pattern.

I   β'-COP^{mGFP} fluorescence foci in Dsl1p-depleted GAL-*DSL1* cells after incubation in glucose-containing medium (YEPD) for 4 h at 30°C.

J   Schematic representation of the characteristic polarized BiFC spot localization during different phases of bud outgrowth. BiFC foci are displayed in black; ER is marked dark gray for orientation.

exhibited polarized BiFC fluorescence at the future bud site prior to bud outgrowth. In the first minutes of discernable bud outgrowth, fluorescence signals remained localized to the bud neck at the side of the mother cell. After that, the fluorescence signals relocated to the bud tip and remained there until apical bud outgrowth ceased. During the phase of isotropic growth, the BiFC signals dispersed throughout the daughter or briefly disappeared altogether. When the daughter cell was pinched off from the mother during cytokinesis, fluorescence signals appeared at the bud neck. In diploid cells, the BiFC spots accordingly relocated to the opposite cellular pole, where the next bud site would form. In summary, signals were found wherever intensive material turnover and membrane outgrowth takes place (Field & Schekman, 1980; Finger *et al*, 1998). This observation has two implications: First, the dynamic behavior of the BiFC-marked interactions appears to allow for a signal to disappear despite an assumed irreversibility of the split-YFP complementation. Second, it shows that the interaction between Dsl complex and COPI subunits is only polarized as long as there is intense material consumption at the bud due to membrane outgrowth. Time-lapse recordings revealed that the polarization is dependent on the ability of the cell to grow, as cells in G$_0$ phase generally exhibited an isotropic punctate distribution of foci throughout the cell, as opposed to budding cells (S. Schröter, unpublished results). Accordingly, glucose-starved cells that had halted growth showed COPI•Dsl signal distribution patterns reminiscent of ER exit site patterns (Fig 2B). This signal localization was reversible: A few minutes after the addition of glucose, polarized distribution of the COPI•Dsl signals had resumed (Fig 2C, Movie EV1). Polarized COPI•Dsl signals were also observed in the emerging zygote of mating cells. Fluorescent signals showed a localization preference toward areas of membrane outgrowth (Fig 2D), similar to those in budding cells. This suggests that the observed interactions reflect a commonly occurring process in the cell that does not depend on for instance the physical barrier between mother and daughter cell during budding (Clay *et al*, 2014). Importantly, the tendency of the BiFC signal to occur in a polarized manner is very much dependent on the chosen BiFC pairs and not generally caused by the tags. While Dsl•Dsl combinations yielded a uniform ER staining (Fig 1D), COPI•Dsl1 and COPI•COPI BiFC combinations resulted either in the polarized staining pattern described above, or in a more random Golgi-like fluorescence pattern (Fig 2E, upper and lower row and Fig 3H). The dynamic behavior of COPI•Dsl BiFC signals is also illustrated by the recovery of the BiFC signals after photobleaching

(Fig 2F and G). Bleaching of COPI•Dsl BiFC signals yielded similar recovery rates independently of whether entire cells, full buds, or only BiFC punctae in buds were bleached (Fig 2F and G). Recovery was detectable after a few minutes and steadily increased over time. The kinetics of the fluorescence recovery under all conditions suggest that it was due to *de novo* formation of BiFC fluorophores, and not due to diffusion or assisted transport of existing fluorophores, which would require only a few seconds (van Drogen *et al*, 2001). Moreover, the data advocate that BiFC complexes originating from the mother cell contribute very little to the formation of BiFC spots in the daughter cell. The comparably fast initial recovery must be due to existing unpaired molecules that finish their maturation after bleaching. This in turn implies that the cells possess adequate amounts of uncomplemented proteins to fulfill the physiological function of the investigated interactions, even if a fraction of the proteins may constantly be removed from the pool of functional proteins through the formation of stable BiFC complexes.

COPI•Dsl BiFC interactions mark ER arrival sites

All COPI•Dsl BiFC pairs showed polarized signal distribution (Figs 3A–D and EV3A). The question remained whether the observed BiFC signals between the Dsl complex and COPI subunits reflect binding of entire vesicles, or whether the Dsl complex interacts with free COPI subunits. We reasoned that if the observed BiFC signal accounted for functional COPI vesicles interacting with the Dsl complex, cargo molecules would be close by and thus able to form BiFC interactions. To test this, we evaluated the formation of BiFC signals between the COPI cargo protein Rer1p and COPI or Dsl complex subunits, respectively.

The combination of ^{VC}Rer1p with Dsl1p^{VN} and β'-COP^{VN} yielded spatially well-defined BiFC interaction signals with a localization pattern identical to the COPI•Dsl BiFC signals (Figs 3E and F, and EV3A). Rer1p is normally found at the Golgi, and a punctate Rer1p signal at the ER will likely arise from Rer1p performing its function of retrieving cargo to the ER via COPI vesicles. Additionally, the BiFC signals obtained with Dsl1^{VN}•^{VC}Rer1p and β'-COP^{VN}•Dsl3p^{VC} complex were so similar in localization and timing that this suggests a common underlying process—the interaction of arriving COPI vesicles with the Dsl tethering complex. Figs 4G and EV3B illustrate that most ^{CFP}Rer1p marked *cis*-Golgi, and only a fraction, which may represent Rer1p transported by COPI vesicles, colocalized with the β'-COP^{VN}•Dsl3p^{VC} BiFC signal.
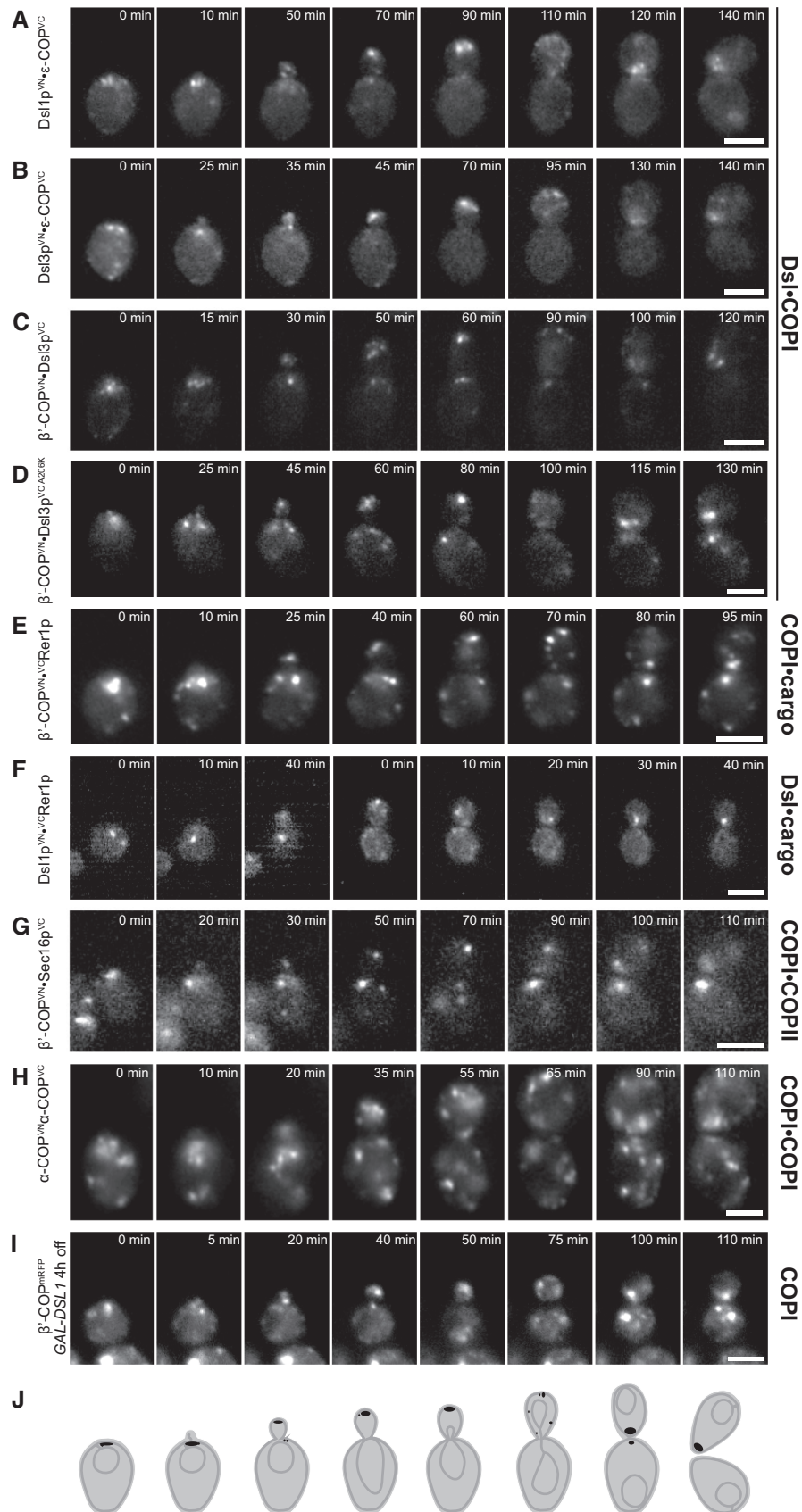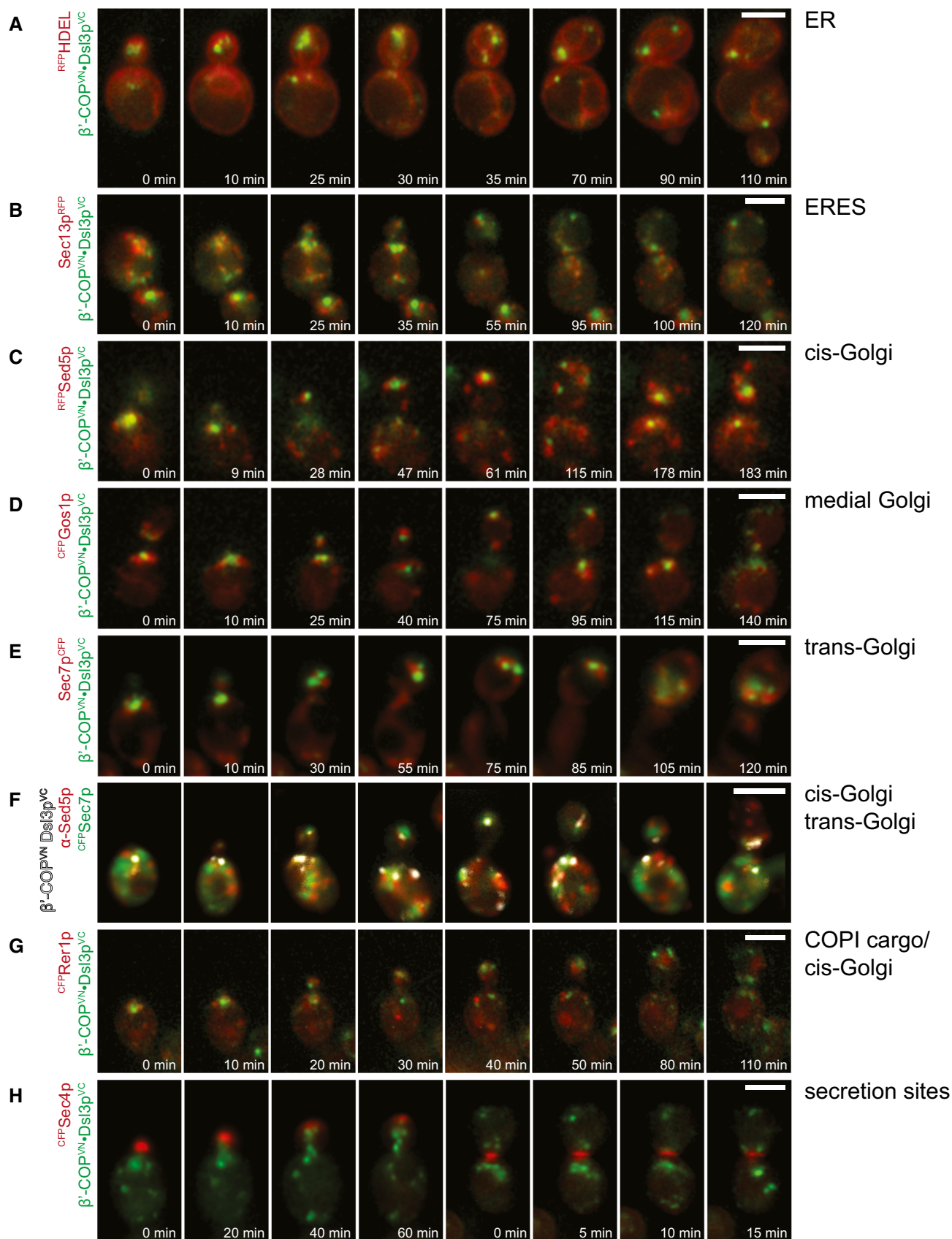
Figure 3.

Figure 4.

Figure 4. Organelle association of β'-COP^{VN}•Dsl3^{VC} BiFC spots.

A–H Time-lapse images of agarose-embedded cells were taken at RT with supply of fresh PM Glc + ura medium throughout one budding cycle. Only panel (F) shows fixed cells immunostained for Sed5p. All cells produced the β'-COP^{VN}•Dsl3p^{VC} BiFC pair. Most strains contained plasmids encoding different organelle markers as indicated below. BiFC signals are pseudocolored green; organelle markers are pseudocolored red. Scale bar, 5 μm. (A) ^{RFP}HDEL, ER marker. (B) Sec13p^{RFP}, ER exit sites marker. (C) ^{RFP}Sed5p, *cis*-Golgi markers (genomic). (D) ^{CFP}Gos1p, *medial* Golgi marker. (E) Sec7p^{CFP}, *trans*-Golgi marker. (F) Individual fixed cells carrying the β'-COP^{VN}•Dsl3p^{VC} BiFC pair along with *trans*-Golgi marker ^{CFP}Sec7p were used for this panel. The β'-COP^{VN}•Dsl3p^{VC} BiFC signals are pseudocolored white. Immunostaining was used to visualize the *cis*-Golgi marker Sed5p (red). The *trans*-Golgi marker ^{CFP}Sec7p is pseudocolored green. (G) ^{CFP}Rer1, COPI cargo. (H) ^{CFP}Sec4p, marker for secretory vesicles.

Strikingly, the reported localization pattern could also be observed independently of the use of BiFC markers. β'-COP^{mRFP} showed polarized localization under conditions of Dsl1p depletion (Fig 3I). The GAL-dependent expression of *DSL1* was halted by transferring the cells into glucose-containing medium, and we followed the effect of the reduction of Dsl1p copies (due to several rounds of duplication) on the behavior of the COPI subunit. While β'-COP alone showed no polarized localization, a strong decrease of Dsl1p caused an accumulated appearance at the sites of high material turnover, similarly to where COPI•Dsl signals were reported. As Dsl1p depletion leads to COPI vesicle accumulation (Zink *et al*, 2009), its reduction presumably causes a drastic decrease of COPI vesicle consumption, resulting in a vesicle accumulation at the COPI fusion sites. This had been overlooked previously, since cells were examined that had lost polarity because of the long *DSL1* shutoff.

Interaction studies using proximity ligation assays (PLA) (Fredriksson *et al*, 2002) point into the same direction. We probed for COPI/Dsl and COPI/ER-SNARE interactions *in situ* using antibodies against COPI subunits as well as the tags of Dsl1p^{2myc}, Dsl3p^{GFP}, ^{GFP}Sec20p, or Sec20p^{myc}, respectively. The assay leads to the generation of a DNA-based fluorescent reporter, provided that the immunodetected proteins are in close proximity. Indeed, COPI/Sec20p^{myc} and COPI/^{GFP}Sec20p strains showed substantial PLA signals with varying pronunciation. Compared to the wild-type control strain that did not carry a tag epitope, COPI/Sec20p^{myc} cells showed fourfold and 28-fold more signals, and a COPI/^{GFP}Sec20p strain showed twice as many signals in three independent experiments (10–60% of the cells overall carried a signal). The PLA signals between COPI and Dsl proteins were less clear-cut. While one COPI/Dsl3p^{GFP} sample showed a pronounced sixfold signal increase, in other repetitions the numbers of cells exhibiting a PLA signal were only minimally different from the wild-type control. Importantly, the localization of fluorescence signals at bud tip and neck was only observed in COPI/Sec20p and COPI/Dsl cells, and not in the control without tags.

Taken together, these observations support the hypothesis that the fluorescence signals formed through BiFC reflect COPI-coated vesicles making contact with the Dsl1 tethering complex. If our interpretation is correct, these sites evoke the concept of ER arrival sites (ERAS), as postulated by Spang (2009, 2012). Although this presents an interpretation, for simplicity we will continue to use the term ERAS to describe COPI•Dsl punctae in the remaining text.

Putative ERAS localize to ER and Golgi structures, and appear juxtaposed to ER exit sites

These findings raised our interest as to why the putative ERAS appear polarized, much in contrast to their evenly distributed counterparts, the ER exit sites (ERES). As the COPI vesicles are derived from the Golgi and arrive at the ER to release their content, the BiFC interaction signals are expected to appear at the donor or acceptor organelles of these carriers. To analyze this, signals of the BiFC pairs β'-COP^{VN}•Dsl3p^{VC} and Dsl1p^{VN}•ε-COP^{VC} were compared to the localization of the ER (^{RFP}HDEL), the ER exit sites (Sec13p^{RFP}), as well as *cis*-, *medial*-, and *trans*-Golgi (^{RFP}Sed5p,^{CFP}Gos1p, and Sec7p^{CFP}, respectively). Time-lapse recordings allowed for an assessment if an observed association was stable, that is, not coincidental.

Endoplasmic reticulum association of the BiFC fluorescence signals was consistent, and time-lapse imaging confirmed a continuous peripheral association of the signals with the cytoplasmic side of ER (Figs 4A, EV3B and EV4A; Movie EV2). ERES were generally found next to the putative ERAS (Figs 4B and EV3B). Conversely, not all ER exit sites exhibited a corresponding BiFC signal, except in cells with dispersed COPI•Dsl BiFC signals (Fig EV4C–E). Sec13p^{RFP} foci appeared more intense near COPI•Dsl BiFC signals.

How tight is the association between the putative ERAS and ERES? A slowdown in ER–Golgi transport either by glucose starvation or by shifting the *sec12-4* mutant to the restrictive temperature reduced the number of Sec13p-positive spots per cell and often left only one bright spot (Castillon *et al*, 2009; Zink *et al*, 2009; Shindiapina & Barlowe, 2010; Okamoto *et al*, 2012). We created a *sec12-4* mutant strain that produces Sec13p^{mRFP} and the β'-COP^{VN}•Dsl3p^{VC} combination. In this strain, bright Sec13p^{mRFP} and the COPI•Dsl BiFC spots did not colocalize after shift to restrictive temperature (Fig EV4B), suggesting different mechanisms behind the coalescence of ERES and the polarization of COPI•Dsl BiFC spots. Meanwhile, evidence for a spatially tight arrangement of COPI and COPII at the ER (as already postulated by Zink *et al* (2009)) becomes apparent in β'-COP^{VN}•Sec16p^{VC} cells that exhibit a polarized punctate fluorescence signals similar to those of COPI•Dsl and COPI•cargo (Fig 3G).

Furthermore, subsets of *cis*-, *medial*-, and *trans*-Golgi compartments were continuously associated with ERAS, and BiFC signals were always found next to Golgi compartments (Figs 4C–E and EV3B; Movies EV3 and EV4). Like ER exit sites, not all Golgi compartments in the cells occurred with a complementing BiFC signal, suggesting that different subsets of Golgi cisternae exist, performing different tasks in the cell. The Golgi subcompartments, which did associate with the ERAS, appeared positioned at opposite sides of the BiFC signals (Fig 4F). We explicitly did not observe a Golgi stacking phenotype. To summarize, it appears that the BiFC spots represent distinct domains that are in close contact with both the Golgi and the ER, marking material exchange hubs between the two organelles.

ERAS follow the exocyst

The bud tip localization of ER arrival sites instigated a possible connection to secretion and the exocyst machinery. To investigate

this, we created and imaged strains with the BiFC pairs β'-COP^{VN}•Dsl3p^{VC} or Dsl1p^{VN}•ε-COP^{VC} and ^{CFP}Sec4p (a small GTPase that associates with exocyst components) as exocyst marker (Walch-Solimena *et al*, 1997). ER arrival sites were found to trail the site of exocytosis at the bud tip (Figs 4H and EV3B). These data hint toward an association of the COPI activity with secretion. We assume that this association is of indirect nature, as the BiFC signal never came very close to the ^{CFP}Sec4p signal or the plasma membrane. Instead, it appeared positioned rather at the periphery of the exocytosis zone.

We also investigated if the lasso domain of Dsl1p plays a role in establishing the polarized localization of the COPI•Dsl BiFC patches. Interestingly, *dsl1-5xWA* mutants exhibiting residual β'-COP^{VN}•Dsl3p^{VC} BiFC fluorescence showed the same polarization patterns as *DSL1* wild-type cells (Figs 5C and 1B). This

suggests that the targeting of the COPI vesicles is not affected by the *dsl1* lasso mutation; however, residence time, proximity, or amount of molecules available for interactions may be compromised.

COPI vesicles are mistargeted in *dsl1* mutants

A clue as to what function Dsl1p performs is given by the effect of the *dsl1-5xWA* mutation on the fluorescence intensity of COPI•COPII BiFC pairs. When analyzing Sec16p^{VN}•α-COP^{VC} and Sec16p^{VN}•ε-COP^{VC} signals, we observed that the brightness of mostly one fluorescent spot was significantly increased in *dsl1-5xWA* mutant cells compared to *DSL1* wild type (Fig 5A and B). This suggests that COPI vesicles can bind to the Dsl complex when the Dsl1p lasso is intact, but make non-cognate contacts with other nearby ER
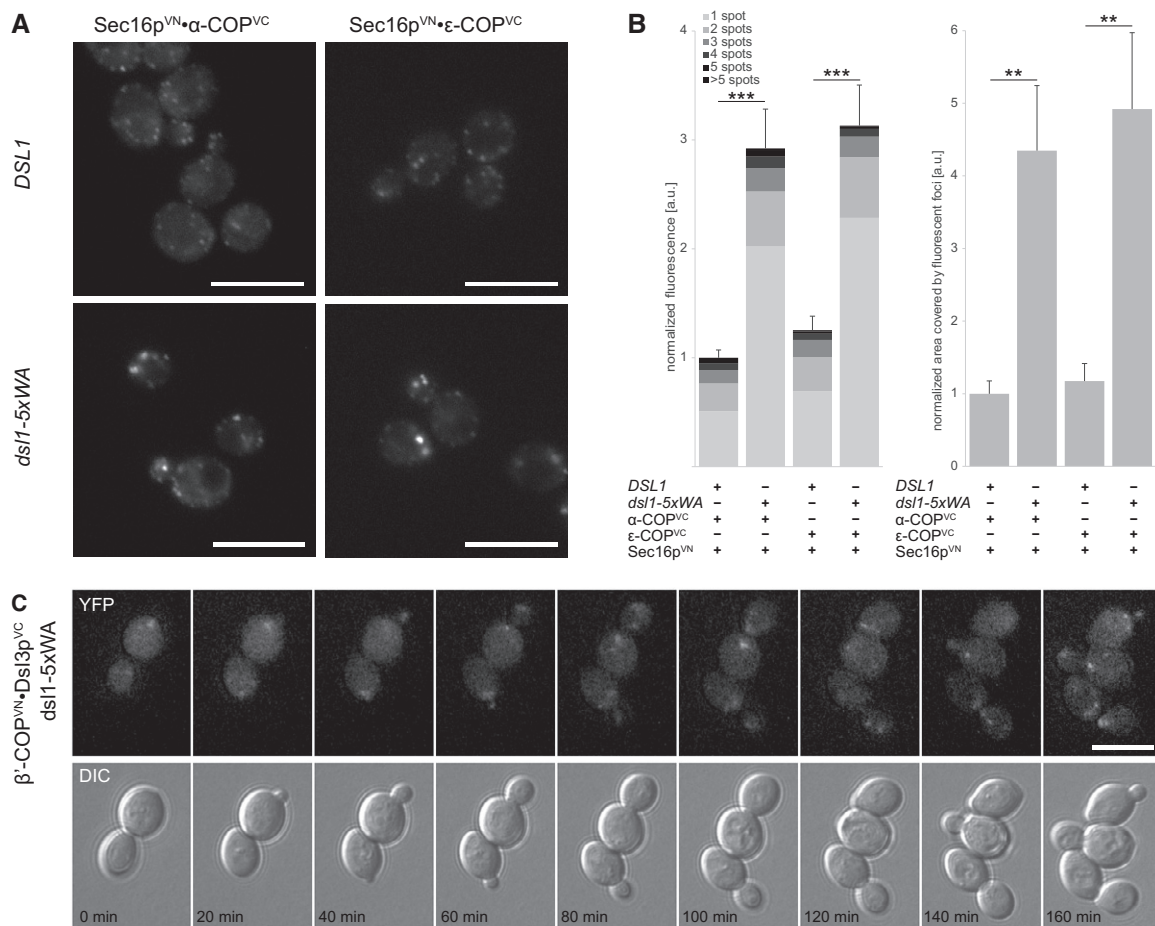

Figure 5. Effects of the *dsl1-5xWA* mutation on COPI•COPII BiFC and COPI•Dsl BiFC.

A Fluorescence micrographs of two different COPI•COPII BiFC pairs are shown: Sec16p^{VN}•α-COP^{VC} or Sec16p^{VN}•ε-COP^{VC}. *DSL1* cells show dispersed punctate patterns resembling ER exit site patterns. In the *dsl1-5xWA* mutant, cells exhibit additional bright spots. Scale bar, 10 μm.

B Quantification of fluorescence intensity differences of the strains shown in (A). COPI•COPII BiFC fluorescence is significantly increased in cells carrying the *dsl1-5xWA* mutant as compared to *DSL1* wild type. Mean values + SEM of at least nine independent experiments ($n = 9–18$) are displayed (two-sample unpaired two-tailed *t*-test; **$P < 0.01$; ***$P < 0.001$).

C Time-lapse micrographs of cells expressing the β'-COP^{VN}•Dsl3p^{VC} BiFC pair in a *dsl1-5xWA* background. Cells were imaged embedded in agarose at RT with fresh PM Glc + ura medium supply throughout one budding cycle. Fluorescence signals retain the characteristic polarization pattern as seen in *DSL1* wild-type cells (see Fig. 3). Scale bar, 10 μm.

proteins when the lasso is mutated. As COPII components of the ERES are in the immediate vicinity of ERAS (Fig 4B) and are locally enriched and far more abundant in copy number in the cell (Wang *et al*, 2015), one can assume that they are available for non-cognate interactions. It was reported that partially uncoated COPI vesicles tend to be "sticky", implying that they bind well to surfaces and each other in an unspecific manner (Rutz *et al*, 2009). Thus, mechanisms must exist that prevent unspecific binding to the ER surface to avoid incorrect alignment with the fusion machinery. It appears that the Dsl complex ensures the specificity of COPI interactions with the ER by acting as a separator that keeps arriving COPI vesicles away from the ER membrane and thereby prevents unspecific and undesired interactions with other ER membrane components.

The polarization of BiFC foci is dependent on actin and the myosin motor protein Myo2p

The COPI•Dsl BiFC signals localize to similar sites as actin patches during growth (Kilmartin & Adams, 1984; Adams & Pringle, 1991). Therefore, the question arose whether the polarization of the BiFC spots is, in fact, actin dependent. We found that the depolymerization of the actin cytoskeleton through latrunculin A indeed led to an even subcellular distribution of BiFC foci (Fig 6A). Before latrunculin A treatment, cells featured one to two bright spots. Minutes after administering the actin-depolymerizing agent, the foci had seemingly dispersed, as six to ten smaller and dimmer spots were visible in each cell. In contrast, the microtubule depolymerizing reagent nocodazole did not have any influence on BiFC signal polymerization (Fig 6B). Careful analysis of the paths of BiFC signal movement in the cell hinted toward a translocation along actin cables, similar to signals described by Schott *et al* (2002) (S. Schröter, unpublished results).

We also tested the involvement of the myosin motors Myo2p and Myo4p on ERAS polarization. We chose these two myosins because Myo2p is responsible for the transport of, amongst others, *trans*-Golgi and secretory vesicles into the bud (Govindan *et al*, 1995; Schott *et al*, 1999, 2002; Rossanese *et al*, 2001). In contrast, Myo4p plays a subtle role in the early steps of cortical ER inheritance (Estrada *et al*, 2003; Schmid *et al*, 2006). Of the two tested myosin mutants, *myo2-66* and *myo4Δ*, only the *myo2-66* mutant strain exhibited unpolarized ERAS foci. In contrast, the *myo4Δ* mutation did not have an effect on ERAS polarization (Fig 6C–E). Interestingly, imaging data with ER and Golgi markers showed that in the *myo2-66* mutant, in spite of loss of polarization, the organelle association of the ERAS was preserved (Fig 6F). This suggests that the ERAS localization is dependent on the localization of the Golgi.

ERAS may form a part of ER–Golgi interaction hubs

Cryoelectron micrographs (Fig 7) with immunogold-labeled COPI coats corroborated the notion that ERAS may appear at sites of material exchange at the ER. The micrographs showed two distinct localizations of COPI coat protein clusters, which can be spatially correlated with the *in vivo* BiFC signals: Antibodies against COPI (Zink *et al*, 2009) recognized areas on aligned membrane structures at the ER of the bud tip or the side of the bud, as well as the bud neck of the mother cell. Labeled structures usually appeared

sandwiched between two membranes, one of which could be identified as ER membrane due to its localization below the plasma membrane or around the nucleus. The data are in line with the hypothesis of the existence of spatially restricted interaction hubs between ER and Golgi, where material is exchanged via vesicular transport.

Discussion

Utilization of the BiFC technique has allowed us to identify possible ER arrival sites in yeast cells by visualizing the interaction sites between the Dsl complex and the COPI coat. This approach has not only established a novel marker to study these sites of COPI vesicle fusion *in vivo*, but it explicitly addresses fusion sites that are active. The results clearly show that dynamic processes occurring at a scale of a few minutes can be visualized by BiFC. The data argue for a direct interaction of the COPI coat complex, either of fully or partially coated vesicles, with the Dsl tethering complex *in vivo*, and imply that COPI vesicles carry their coat when arriving at the ER (Zink *et al*, 2009). Using BiFC, we also found evidence for the importance of the interaction between COPI coat and Dsl complex for cell viability: *dsl1* mutations were lethal when combined with COPI encoding genes, which carried a VN tag or an RFP tag that forms tetramers. These VN combinations became viable again when complementary BiFC-tagged Dsl proteins were provided. Any tested COPI•Dsl combination could suppress the synthetic growth defects, while no other tested VC-tagged genes rescued the lethal COPI^{VN}/*dsl1* mutant combinations. This suggests that the COPI•Dsl BiFC complexes represent a synthetic bypass for the COPI^{VN}/*dsl1* double mutants, and therefore, the COPI•Dsl BiFC complexes reliably recapitulate the physiologically important COPI/Dsl interaction. It also implies that only the successful interaction itself is relevant for cell viability, and that the binding mechanism is of minor importance.

We observe polarized punctate appearance of COPI•Dsl interactions. They are located near exocytic hotspots, and their buildup is most evident in fast-growing cells. Polarized localization was also observed for COPI•COPII, COPI•cargo, and Dsl1p•cargo BiFC pairs and is supported by complementary approaches (COPI/Dsl and COPI/ER-SNARE PLA; COPI localization during Dsl1 depletion).

FRAP data (Fig 2F and G) suggest that COPI•Dsl BiFC complexes form at the site where we report them. Additional arguments speak against the alternative hypothesis that the signal pattern is caused by mislocalization or transport after complex formation: (i) The ER-localized Dsl complex is in a tight complex with three membrane-anchored SNAREs (Kraynack *et al*, 2005; Ren *et al*, 2009; Fig EV1I). This implies that complemented BiFC pairs would require a very efficient transport of the entire SNARE-Dsl-coat BiFC complexes laterally trough the membrane, where they would encounter diffusion barriers in the cortical ER and nuclear envelope at the bud neck (Shcheprova *et al*, 2008; Clay *et al*, 2014). Additionally, Donovan and Bretscher (2015) reported that tethered secretory vesicles are quite immobile. Furthermore, COPI•Dsl BiFC spots likely do not represent aggregates that need to be sequestered, as they (ii) do not colocalize with an autophagosomal marker and are not exaggerated in mutants carrying a defect in autophagy; and (iii) are concentrated in the bud, while the aggregated proteins stay in the mother cell and are actively translocated
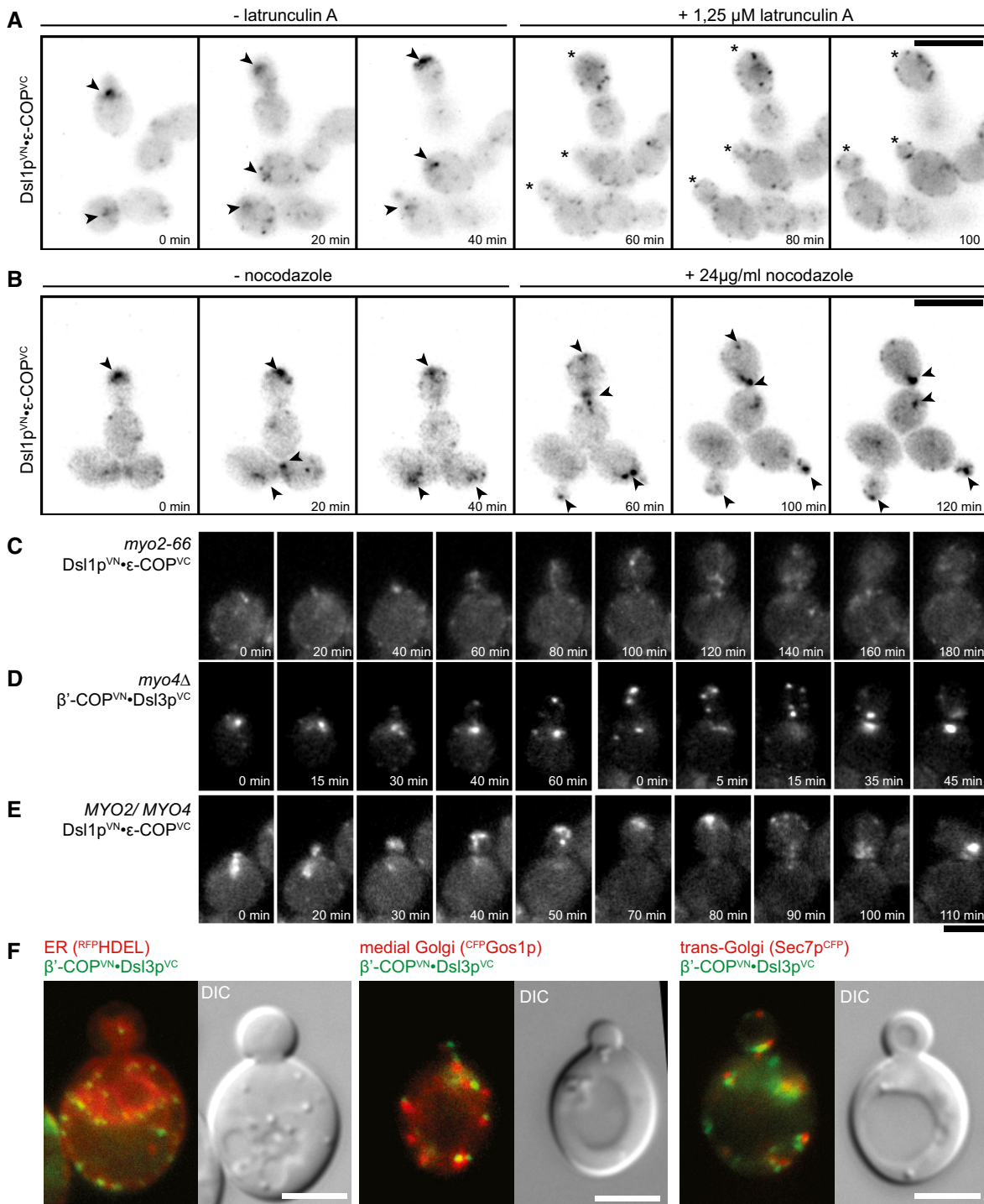
Figure 6. Dependence of ERAS distribution on cytoskeletal structures.

A, B   Involvement of filamentous cytoskeletal structures in COPI•Dsl BiFC foci polarization. Time-lapse micrographs of agarose-embedded cells expressing the Dsl1p^{VN}•ε-COP^{VC} BiFC combination at RT with fresh PM Glc + ura medium supply. (A) Upon disruption of actin filaments with 1.25 μM latrunculin A, COPI•Dsl BiFC signals dispersed. (B) Microtubuli disruption through 24 μg/ml nocodazole did not affect polarization of the COPI•Dsl BiFC signals. Arrowheads: polarized signal, asterisks: unpolarized localization. Fluorescence images are displayed with inverted brightness values. Scale bar, 10 μm.

C–E   Involvement of myosin motors in BiFC foci polarization. Time-lapse micrographs of agarose-embedded cells carrying the COPI•Dsl BiFC pairs Dsl1p^{VN}•ε-COP^{VC} or β'-COP^{VN}•Dsl3p^{VC} were taken. Either wild-type cells (E) or mutants carrying the myosin V mutations *myo2-66* (C) or *myo4Δ* (D) were analyzed. Cells were grown at RT with fresh PM Glc + ura medium supply. In the *myo2-66* cells, the BiFC signal polarization was hardly detectable even at permissive temperature, while it was unaffected in *myo4Δ* compared to the control cells. Scale bar, 5 μm.

F   Fluorescence micrographs of β'-COP^{VN}•Dsl3p^{VC} cells carrying the *myo2-66* defect. COPI•Dsl BiFC, and ER or Golgi markers were analyzed. While the BiFC spots were dispersed in these mutants, they retained their association with ER and Golgi. Scale bar, 5 μm.
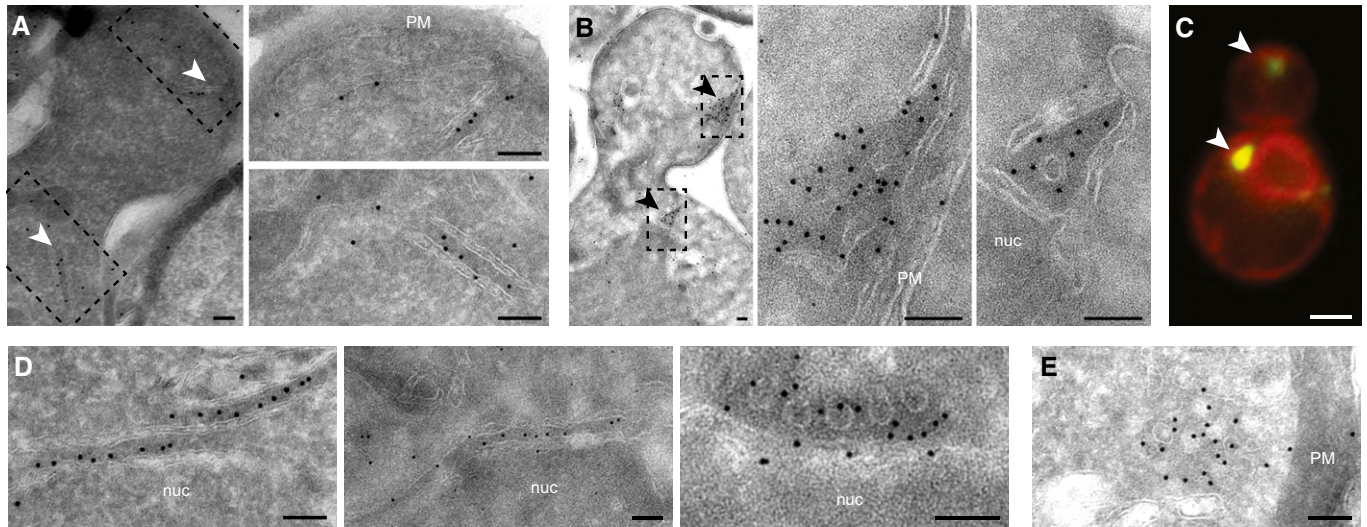
Figure 7.   Subcellular localization of COPI•Dsl interactions in immuno-electron microscopy.

A, B   Immuno-electron micrographs showing the buds and the neck region of two β'-COP^{VN}•Dsl3p^{VC} cells. Both parts contain an overview image (left) and two zoomed details (right). Slides were decorated with antibody against COPI and visualized with protein A-conjugated 10-nm gold particles. Gold particles mark electron-dense areas in apposition to membranes and/or vesicular structures (arrowheads), which are localized at the side of the bud and the bud neck of the mother cell. PM: plasma membrane, nuc: nucleus. Scale bar, 100 nm.

C   Fluorescence micrograph of a budding cell carrying β'-COP^{VN}•Dsl3p^{VC} (green) and ^{RFP}HDEL (red). Arrowheads mark BiFC signals which may correspond to the localizations found in (A) and (B). Scale bar, 2 μm.

D   COPI-positive, electron-dense structures in close apposition to perinuclear ER; 10-nm gold particles mark COPI. nuc: nucleus. Scale bar, 100 nm.

E   Accumulation of COPI-positive vesicles; 10-nm gold particles mark COPI. PM: plasma membrane. Scale bar, 100 nm.

from the daughter to the mother (Kaganovich *et al*, 2008; Liu *et al*, 2010; Denoth Lippuner *et al*, 2014). The sum of evidence, together with the proper method controls, leads us to conclude that the BiFC interactions reflect active COPI vesicle fusion sites, or ER arrival sites (ERAS).

Admittedly, the finding that a presumably constitutive retrograde trafficking route would converge at virtually one spot at the ER is quite surprising. In the next paragraphs, we aim to provide an intuitive interpretation for this observation (see also Fig EV5A). The fusion sites of COPI vesicles in yeast are dependent on the localization of the Golgi as their donor organelle, as the vesicles rely on diffusion in yeast (Barlowe & Miller, 2013). Interestingly, we found a dependence of the putative ERAS on the motor protein Myo2p and an intact actin cytoskeleton, both of which are also responsible for the polarization of certain Golgi substacks (Rossanese *et al*, 2001). We reason that the mechanism underlying the polarized delivery of COPI vesicles may in fact be that of directed Golgi localization toward the ER. Indeed, our EM images show COPI of COPI•Dsl BiFC strains sandwiched between morphologically regular ER a second membrane that may represent Golgi. Curiously, it was also shown before that yeast δ-COP binds Myo2p via the small GTPase Ypt11p, and that this contributes to *trans*-Golgi inheritance (Arai *et al*, 2008). However, we saw no abolishment of β'-COP^{VN}•Dsl3p^{VC} signal polarization in *ypt11Δ* strains (H.D. Schmitt, unpublished results). This speaks against an involvement of Ypt11p in the localization of ERAS.

We report that ERAS associate with a subset of ER exit sites. COPI•COPII BiFC signals indicate that neighboring ERAS and ERES indeed share contact sites. But why are COPI•Dsl and COPI•COPII BiFC signals distributed asymmetrically over the ER while the

majority of ERES are not? The explanation may lie in the discovery that different subtypes of ER exit sites exist. ERES gather different cargo molecules, become dimmer or cluster together, and respond differently to increasing cargo load (Farhan *et al*, 2008; Castillon *et al*, 2009; Shindiapina & Barlowe, 2010). In line with this, we interpret our observations in the way that COPI•COPII BiFC may in fact reflect active ERES that experience incoming traffic from their adjacent ERAS. In contrast, ERES, which do not have corresponding active ERAS, may be ones that are dormant. Conversely, we assume that ERAS will form an ERES-like pattern under certain growth conditions (Fig 2B), but the ERAS at the bud tip is by far the most active during polarized growth.

We observe ER, *cis*-Golgi, ERAS, and ERES all in close proximity (Fig EV5C). This suggests that they may all be part of an ER–Golgi interaction hub, where forward and retrograde transport routes converge in a cycle of trans-organelle and lateral intra-organelle transport between ER and Golgi (Fig EV5D). This design would maintain efficient material exchange through short distances, while keeping subdomains organized and separated. Indeed, a number of findings from other research laboratories are consistent with the notion of the existence of an ER–Golgi interaction hub. Several organisms exhibit a tight association of *cis*-Golgi and ER exit sites (Whaley *et al*, 1975; Farquhar & Palade, 1981; Rossanese *et al*, 2001; Bevis *et al*, 2002; daSilva *et al*, 2004; Lerich *et al*, 2012). In mammalian cells, where Golgi and ER are further apart, the vesicular tubular clusters (VTC) or ER–Golgi intermediate compartment (ERGIC) are close to the ER exit sites (Bannykh *et al*, 1996; Appenzeller-Herzog & Hauri, 2006). Along the same lines, retrograde cargo in mammalian cells is directed to ER exit sites (Mardones *et al*, 2006), and retrograde transport was shown to be

involved in the formation of ER exit sites (Ronchi *et al*, 2014). In *Saccharomyces cerevisiae*, where the Golgi compartments are not stacked, the *cis*-Golgi compartment is temporarily associated with the ERES (Levi *et al*, 2010; Kurokawa *et al*, 2014). It has been shown that a prolonged presence of COPII coat on vesicles promotes ERES-*cis*-Golgi association (Kurokawa *et al*, 2014). The presence of COPI coat on vesicles may favor a tight association of *cis*-Golgi and ERAS in an analogous way.

It is even conceivable that ER–Golgi interaction hubs are part of a higher order cellular structure, in which the endocytic and exocytic pathways are arranged in an antiparallel fashion. At the tip of the yeast bud, sites of endocytosis appear in a ring-like pattern around the area of maximal exocytosis (Kohli *et al*, 2008; Jose *et al*, 2013, 2015). Since polarity factors like Cdc42p also cycle by vesicular transport, this arrangement helps to establish cell polarity (Watson *et al*, 2014). Careful inspection of our BiFC signals revealed that they were often located off the center of the bud, and lateral to exocyst components. In accordance with this, we have observed ring-like COPI•Dsl BiFC structures on a number of occasions. Our results suggest that the parallel arrangement of secretory pathways may extend inward from the site of most active exocytosis to the ERES. This interpretation is consistent with the notion that tethering factors may present factors for the underlying ability of the endomembrane system for self-organization (Glick, 2014). The antiparallel design of exocytic and endocytic membrane elements may guarantee that all necessary parts of the secretory machinery are transferred to the new daughter cells in a coordinated fashion.

With that in mind, the observed bud-focused COPI transport can be interpreted to play a role in the inheritance of Golgi to the bud (Fig EV5B and C). It has been reported that *trans*-Golgi membranes enter the bud of a growing yeast cells in a Myo2-dependent fashion (Rossanese *et al*, 2001), while the *cis*-Golgi forms *de novo* by fusion of COPII vesicles that are formed from ER that has been pulled into the bud from the mother cell (Reinke *et al*, 2004). The positioning of ERAS between ERES and Golgi elements may enable retrograde transport from the *trans*-Golgi via the ER to contribute to the formation of *cis*-Golgi elements in the bud. High-resolution 3D imaging may help shed more light on their precise association and positioning in future works.

A possible function of the Dsl complex as a factor in ER organization can be deduced from BiFC experiments with the COPII recruitment factor Sec16p in *dsl1* mutant background. While the *dsl1-5xWA* mutation reduced the COPI•Dsl interaction, it led to a significant increase in the BiFC signal intensity between COPI subunits ε-COP^{VC} or α-COP^{VC} and COPII factor Sec16p^{VN}. Similar results were obtained using the *dsl1-22* mutant (S. Beckmann, unpublished results). This indicates that, in the absence of an intact Dsl1 binding site, COPI subunits are more likely to approach non-cognate interactors at the ER membrane. These findings are in line with a previously described targeting defect in a mutation in the third subunit in the Dsl complex, Tip20p: In a cell-free assay with membranes from a *tip20-8* mutant as acceptor, COPII vesicles fuse back with the ER (Kamena & Spang, 2004). In contrast, the function of the Dsl complex does not seem to lie in the polarized delivery of COPI vesicles, since β'-COP^{VN}•Dsl3p^{VC} and β'-COP^{VN}• Sec16p^{VC} BiFC spots retained their polarized localization pattern in *dsl1* mutants (Fig 5). Since the Dsl complex is distributed evenly across the ER, the emerging picture points toward a possible function as a gatekeeper, where the Dsl complex assures that COPI vesicles will be reliably tethered, no matter where at the ER they arrive. By preventing COPI vesicles from approaching the ER membrane in an uncontrolled manner, it may prevent non-cognate contacts with nearby ER proteins, which would possibly present a non-fusogenic dead-end state for the respective COPI vesicles. In this, it may be involved in keeping ERAS and ERES spatially separated in a fashion very similar to the exocyst, where exocytic and endocytic domains at the plasma membrane are kept separate (Jose *et al*, 2015). Besides the Dsl complex, there are at least two other proteins or complexes that are evenly distributed across an organelle but active at specific sites only. These are Sec12p, the GTPase involved in COPII vesicle budding, and the Q/t-SNAREs Sso1p and Sso2p at the plasma membrane (Brennwald *et al*, 1994; Sato *et al*, 2003).

The emerging picture is that healthy growing yeast cells may show their highest COPI transport activity at a Golgi element localized to the bud tip, which creates the appearance of a mainly bud tip focused COPI transport. COPI vesicles are received by the evenly ER-distributed Dsl complex (thereby creating an ER arrival site), which prevents them from coming into too close contact with nearby ER exit sites (Fig EV5A).

In summary, the *in vivo* results presented in this work confirm that COPI vesicles arrive at the ER while still coated. Genetic data indicate that the interaction of the vesicle coat with the ER-resident Dsl1 tethering complex is substantial for cell viability. The Dsl complex carries out a discrimination function at the boundary of COPI and COPII rich domains of the ER. It appears to be important for capturing COPI vesicles by their coat, and guiding them toward controlled fusion. The interaction of COPI components and the Dsl complex appears to occur at specialized ER arrival sites. In fast-growing cells, ER arrival sites occur at rapidly expanding plasma membrane regions. Since they are close to ER exit sites as well as Golgi membranes, they may be part of a larger hub for material transfer between these organelles. The role of COPI transport in the growing bud may be to maintain the distribution of cycling factors and maintain membrane homeostasis by balancing the massive exocytosis events at the bud. The process could function even as a delivery mechanism for Golgi material to the bud. It will be an interesting challenge to investigate more closely the factors that regulate ERAS localization and to find further evidence on the function of the observed polarized COPI transport. We are also aware that the proposition that COPI vesicles arrive at the ER in a coated state opens new questions as to what factors and by what mechanisms coat removal is initiated and carried out. Future work will have to elucidate in more detail the role of the Dsl complex in these processes, as well as by what means it may carry out its discriminating function, and by what mechanisms it is involved in uncoating.

Materials and Methods

Yeast strains and growth conditions

Yeast strains used in this work are listed in Appendix Table S1. Strains without plasmids were grown in YEPD (2% Peptone, 1%

yeast extract, 2% glucose, 20 mg/l uracil), while those carrying plasmids with *URA3* marker were grown in PM medium, an synthetic minimal medium (0.67% yeast nitrogen base; Formedium, Hunstanton, UK) with 2% glucose and 0.5% peptone from casein (Applichem, Darmstadt, Germany). Selection for *LEU2* containing plasmids was performed using a synthetic complete medium lacking leucine but containing all other amino acids plus uracil and adenine (arginine, histidine, methionine, cysteine, uracil, and adenine 20 mg/l; lysine, tyrosine 30 mg/l; tryptophan 40 mg/l; phenylalanine 50 mg/l; leucine 60 mg/l; alanine, aspartic acid, glutamic acid, serine, threonine, valine, 100 mg/l). A similar medium lacking methionine and cysteine instead of leucine was used for labeling of cells with ^{35}S-labeled amino acids. Pre-cultures of strains used for live-cell imaging were grown over night in YEPD or PM medium to densities below $OD_{600} < 1$ and kept at an OD below 1 by diluting them in fresh medium over the day if necessary. For sample preparation, cultures were always taken fresh out of the incubator. Growth assays were performed with cells growing overnight on YEPD plates (Fig EV1G) or SC plates with galactose as carbon source lacking leucine (Fig EV2, Appendix Fig S1). A loop of cells was transferred into liquid YEPD medium. After 4 h growth in YEPD at 30°C, cell density was determined and adjusted to 1 OD_{600}. Serial dilutions were plated on galactose or glucose-containing media plates, and plates were incubated at different temperatures as indicated.

Antibodies, immunoblotting, and TAP purification

Sera against the yeast COPI complex were a gift from Anne Spang (Basel). Polyclonal antiserum against δ-COP (Ret2p), ε-COP (Sec28p), Emp47p, and hexokinase were raised by Dr. Stephan Schröder-Köhne, while he was working at our institute. Monoclonal mouse myc-tag antibody 9B11 was purchased from Cell Signaling Technology, Danvers, MA. Immunoblotting was always performed with extracts made from the equivalent of 5 OD_{600} units of cells. After collecting cells and washing with water, cells were lysed in 2 M NaOH + 5% mercaptoethanol, and proteins precipitated with 10% trichloroacetic acid. The pellet was neutralized with 1.5 M Tris base and dissolved in SDS sample buffer. Proteins were separated using 8% SDS–PAGE. For Rer1p blots, we used 10% SDS–PAGE. The tandem affinity purification of the Dsl complex was performed as described by Kraynack *et al* (2005). For the two affinity purification steps, we employed mouse IgG and calmodulin conjugated to magnetic beads (New England Biolabs, Ipswich, MA and bioWORLD, Dublin, OH, respectively). The calcium concentration in the buffer used for the second purification step was 2 mM. Proteins were boiled off the beads in sample buffer.

In situ antibody staining for immunofluorescence and PLA was carried out on cells that had been fixed on poly-L-lysine-coated glass slides with 3.5% paraformaldehyde solution in PBS buffer containing 1.2 M sorbitol. Cells were decorated with 1:5,000 COPI serum (see top of the paragraph), antibodies against Sed5p (immunostainings), or monoclonal antibodies against the myc epitope (9B11 1:1,000–1:8,000, NEB) or GFP (GF28R, 1:1,000, Thermo), respectively. PLA protocol was carried out according to manufacturer's instructions with a Duolink® *In Situ* red kit from OLINK Bioscience, Uppsala, Sweden.

Genomic tagging

Segments encoding BiFC tags were fused in frame to the 3′ end of various yeast genes at their genomic loci by a PCR-based gene targeting approach. PCR was performed with vectors as template that are listed in Appendix Table S2 (Sung & Huh, 2007). The used oligonucleotides can be found in Appendix Table S3 (oligonucleotide 1–24). To improve the yield of positive transformants, we often used strains that already carried a modification of the gene of interest along with the His3MX marker at the 3′ end of our genes of interest (Ghaemmaghami *et al*, 2003; Huh *et al*, 2003). In this case, the same reverse primer derived from the TEF terminator sequence could be used for all replacements that involved the KanMX6 cassette for the selection of transformants (oligonucleotide 1). The in-frame fusion of the tags was checked by PCR and sequencing using the primers 25–42. For the introduction of the VC tag in front of the *RER1* gene, a second PCR was performed to extend the region of homology at the end of the PCR products using primer 23 and 24. A segment coding for a five-residue glycine-rich linker region (GGSGT) lies between the VC and the *RER1* sequences. After the successful insertion, PCR and sequencing indicated that we had obtained a vector that contained the strong *RPL1B* promoter instead of the weaker *CET1* promoter in front of the 5′ VC sequence. In spite of several attempts, we were not able to insert the weaker promoter in front of the VC-*RER1* fusion. To avoid problems caused by a possible overexpression of the VC-*RER1* construct, we used an *rer1* deletion strain that contains a VC-tagged version of *RER1* expressed from a plasmid (p316-^{VC}RER1). This construct is under the control of the *RER1* promoter, and the codon usage of the VC-encoding segment had been adapted to that of *S. cerevisiae*. The intensity of BiFC spots and their localization were indistinguishable. However, the cells expressing the plasmid-encoded version were not temperature-sensitive even on selective minimal medium, while the genomic *RPL7B* regulated version rendered the cells temperature-sensitive in combination with various VN-tagged genes (Fig EV1H). The disadvantage of working with the plasmid-encoded version was the fact that almost 20% of the cells expressing plasmid-encoded VC-*RER1* lacked any fluorescence due to plasmid loss. Cells may survive the loss of the plasmid even on media selecting for the biosynthetic marker since *RER1* is not essential.

To reconstitute a monomeric form of YFP by the BiFC approach, p^{mVC}TRP was used as a template for the PCR dependent tagging of the *DSL3* gene. This plasmid harboring a mutation equivalent to the A206K mutation was obtained by PCR with p^{VC}TRP as template and the primers 43 and 44. This PCR created a silent BlpI site, which was used for cleavage followed by ligase-catalyzed ring closure. Similarly, the I152L mutation was introduced into the VN fragment by PCR using p^{VN}TRP as template and primers 45 and 46. A silent BssHII site was created by this PCR. Cleavage and ligase-catalyzed ring closure created p^{VNi152l}TRP, which was used for PCR to introduce the low background mutant version of VN 3′ of the *SEC27* (β'-COP) gene. The lasso-encoding region was deleted from the chromosomal copy of *DSL1* first by a pop-in–pop-out approach. The region was deleted from p306-d1-5WA by PCR using the primers 51 and 52. By cleaving the PCR product with AscI and ligase-catalyzed ring closure, codon 378–488 of *DSL1* were replaced with a short

linker (GGC GCG CCC). After sequencing, the plasmid was cleaved with SnaBI to direct its insertion 3′ of the *DSL1* locus in a *dsl1::KanMX* strain. This strain contained a *HIS3* plasmid carrying a wild-type version of *DSL1*. After transformation, we screened for clones that survived the loss of the plasmid. After crossing with BiFC strain XII-27, Ura$^+$ spores were plated on 5-FOA containing plates. A resulting 5-FOA$^+$ clone (XVI-7) and the 5-FOA$^-$ strain (XVI-6) were analyzed by PCR using three pairs of *DSL1*-specific primers to verify the correct integration.

TAP-tagged and myc-tagged versions of different *DSL1* alleles (Fig EV1B and H) were obtained by first amplifying the tagged chromosomal *DSL1-TAP::His3MX* and *DSL1-6His-2myc::KanMX* alleles from strain YSC1178-7502517 or YUA1, respectively, and using primers 48 and 49. The PCR products were used for transformation into the *dsl1-5xWA* and *dsl1-Δlasso* mutants.

To obtain *dsl1-5xWA* mutants harboring different BiFC pairs, we made crosses producing either heterozygous diploids which were either *dsl1-5xWA*/GAL-DSL1 or *DSL1*/*dsl1-5xWA*::pRS306-dsl1-5xWA. Since the *dsl1-5xWA* mutation has little effect on growth, we utilized the *URA3* marker to confirm the presence of the mutation in spores derived from various crosses. The presence of a second copy of this mutation had no effect on the results (data not shown). A *SEC27*$^{VN-tagged}$ version (β′-COP^{VN}) with NatMX marker instead of KanMX marker was created by transformation of strain XVII-1 with a PCR product obtained with pRS408 as template and the primers 60 and 61. yEmCFP was introduced downstream of the *DSL1* gene in strain XVII-2 by amplifying the yEmCFP::caURA3 cassette in vector pKT212 (Appendix Table S2), using the primers 62 and 63 (Appendix Table S3).

Construction of plasmids

Some growth assays were performed with VN- and VC-tagged versions of *DSL1* and *dsl1-5xWA* that were expressed from the centromeric vector pRS315 (see Figs 1E and EV2). XbaI and NotI restriction sites were created by PCR in front of the VN and VC sequences and at the end of the ADH1 terminator using p^{VN}TRP and p^{VC}TRP and primers 47 and 48 or 47 and 49. The PCR products were first cloned into pCR2.1-TOPO for control sequencing and then transferred as XbaI-NotI fragments into vector pUA73 (pRS315-*DSL1*) and p315-d1 (pRS315-*dsl1*-5xWA), taking advantage of a naturally occurring XbaI site close to the stop codon of *DSL1*. Along with the BiFC tags, this cloning steps introduced the ADH1 terminator region into the plasmids 11–14 (Appendix Table S2), thereby replacing 450 residues downstream of *DSL1*.

The plasmid p^{CFP}RER1 was obtained as follows: A 960-bp PCR fragment carrying an XhoI and a BglII cleavage site at its ends was created which contains the GPD1 promoter in front of CFP(cerulean)-encoding sequences. For this PCR, we used plasmid p^{CFP}SEC4 (Gitler *et al*, 2009) as template and primers 53 and 54. The XhoI/BglII cleaved PCR product was inserted in front of the *RER1* gene in a XhoI-BamHI cleaved pRS316-based p^{GST}RER1 plasmid. (This cleavage removes the CYC1 promoter and GST tag in front of *RER1*.) The start codon of *RER1* in pRS316-CYC1^P-GST-*RER1* is immediately downstream of a BamHI site. The plasmid also includes 231 bp 3′ of the stop codon of *RER1*.

The E2 crimson version of RFP carrying the N- and C-terminal ER targeting sequences of the Kar2 protein was expressed from the centromeric vector YCplac33. The sequence encoding the chimeric protein along with the TPI promoter and the CYC1 terminator region were excised from plasmid YIplac204 TKC-E2-crimson-HDEL (Strack *et al*, 2009) with KasI and HindIII and transferred into the YCplac33 that was cleaved by the same enzymes.

As described above, the N-terminal tagging of *RER1* was difficult. A plasmid-encoded version of ^{VC}RER1 was generated by gene synthesis (Eurofins) which included the intergene region between the RER1 and the reading frame upstream of *RER1* and the VC fragment with codon usage adapted to *S. cerevisiae*. The VC sequence starts with Met-Asn-His-Asp, where the last residue corresponds to residue 155 of the YFP. A polylinker encoding the segment Gly-Ser-Gly-Gly-Ser ends with a BamHI site. The XhoI-BamHI fragment with these two segments was inserted in front of the *RER1* sequences in a pRS316 vector, where a BamHI lies immediately upstream of the RER1 start codon. The insert ends 231 bp downstream of the *RER1* gene.

Fluorescence microscopy, time-lapse imaging

Live cells were pelleted at 90 *g* for 2 min and washed once in PM with glucose or galactose as carbon source + 20 mg/ml uracil (PM Glc + ura/PM Gal + ura) in order to reduce background medium fluorescence. Supernatant was removed, and cells were resuspended in remaining liquid by slurring with a pipet tip. For slide preparation, 10 μl of cell suspension was streaked onto an object holder and covered with a 24 × 60 mm cover slip. Then, the object holder was flipped over and firmly and evenly pressed onto a tissue to create a cell monolayer. The slide was used for no longer than 5 min after preparation. For time-lapse imaging, 5 μl of the cell suspension was mixed with 45 μl of warmed 1% low melt agarose in PM medium containing 2% glucose and 20 mg/ml uracil (PM Glc + ura) at 30°C, then spotted onto a 18 × 18 mm cover slip. The cover slip was glued into the time-lapse chamber using dental molding. All subsequent steps were carried out swiftly to avoid drying out of agarose spots. The time-lapse chamber was glued onto a cover slip with dental molding and immediately flooded with PM Glc + ura medium. After complete curing, the setup was connected to the medium reservoir and waste container, and medium flow was regulated by gravity flow to a flow rate of 100 μl/min. Display details were chosen from the edges of agarose drops, where cells were homogenously in one focal plane and only partially immersed in agarose, leaving a part of the cell exposed to medium.

Imaging was carried out at RT using an Axioimager D1 microscope (Zeiss); a Uniblitz VMM-D1 controller (Uniblitz Shutter Systems); an Axiocam MRm camera (Zeiss); an Plan-Apo 100x1.4NA or a Plan-Apo 63x/1.4NA oil immersion objective (Zeiss); the filter sets RFP 00, GFP 13, CFP 47, YFP 46 (Zeiss); and the Axiovision AxioVs40 4.8.2.0 software (Zeiss). Light source was a Lumen 200 lamp (Prior).

FRAP experiments of Venus BiFC strains were carried out on a ZEISS Observer Z1 with LSM 780, LCI Plan-Neofluar 63x/1.3 Imm Korr DIC M27 objective. Bleaching was carried out at maximum pixel dwell time for three repetitions of 100% laser intensity in pre-defined ROIs. Images were either acquired in single plane or as z-stack, of which the slice of the bleached cell center was selected prior to image analysis.

Electron microscopy

Electron microscopic imaging was carried out in collaboration with Dirk Wenzel of the Electron Microscopy department of our institute. Cultures were grown o/n at 30°C in YEPD to 1 OD_{600} and harvested (10 min 700 *g* RT). Cells were washed once with YEPD and once with fixing solution containing 2% (w/v) paraformaldehyde in PBS. Then, cells were incubated in fixing solution for 30 min at RT. The following treatment was carried out as described by Tokuyasu (1980). Samples were cut into 75-nm-thin slices and decorated with 1:50 solution of anti-COPI antibody (rabbit polyclonal from purified COPI coat, provided by Anne Spang/Rainer Duden; see also Zink *et al* (2009)). The antibody was detected with 10-nm gold-conjugated protein A.

Image data analysis

Qualitative image processing was carried out using MacBiophotonics ImageJ 1.48b software (http://rsbweb.nih.gov/ij/plugins/mbf/index.html, link acquired 02.10.2013). Time-lapse image stacks were corrected for xy-shifts, using the "image stabilizer" plug-in (http://www.cs.cmu.edu/∼kangli/code/Image_Stabilizer.html, link acquired 02.10.2013) and aligning by the DIC channel. Image brightness of time-lapse series was adjusted to compensate for bleaching effects of repeated image acquisitions. Single-cell kymographs were generated by concatenating the central section of the cell (sliced along the pole axis, frames at the width of the bud neck) of a time-lapse dataset (Fig EV3). Quantitative analyses were carried out using Cell Profiler 2.0 (r11710) software (Kamentsky *et al*, 2011). To identify cells, differential interference contrast (DIC) bright field images and UV light of the respective display detail were used. Two CellProfiler pipelines were created. A first pipeline was used to determine the background brightness of each image. Each DIC image was processed by the RescaleIntensity and the Smooth software modules. The EnhanceOrSupressFeatures(DIC) and FindPrimaryObjects modules allow to determine the rough cell localizations. The determined cell areas were enlarged by eight pixels, and data were used to create a negative mask. This mask was used to determine the average brightness of the background of each YFP image, which were averaged, and correction factors were calculated to correct the images for possible illumination variations during an experiment. The correction was performed using the Multiply command of ImageJ. In addition, the background brightness was used to calculate the thresholds for BiFC spots counting in the following step. The BiFC fluorescence intensity was determined by counting spots in the cells using a series of increasing thresholds (progressive thresholding analysis). For threshold calculation, the background brightness plus standard deviation was set as 1 (this value was found to be suitable to identify cells in YFP images in our initial attempts to run CellProfiler). The spot counting pipeline employed a cell identification module, similar to the first CellProfiler pipeline as described above. The exact outlines of the cells were determined by using UV images, which show overall cell shape through unspecific blue UV induced fluorescence of the cells. The FindPrimaryObjects module, which was used to identify the cells, assigned numbers to each cell and larger bud. With a second FindPrimaryObjects command, which applied increasing thresholds, spots were counted. Data output was processed using Microsoft Excel. The mean values for spot numbers and fluorescence coverage per cell were integrated over the obtained threshold values. With this processing method, relative differences between fluorescence spot numbers and foci size were acquired. For data representation, the values of a reference condition were normalized to 100% or 1, respectively. This is for representation purposes only and does not infer that the reference strain carried 100% fluorescence-positive cells. Results from at least three experiments, some involving different isogenic samples, were displayed graphically with standard error of the mean. Statistical analyses were carried out using unpaired, heteroscedastic *t*-test.

Fluorescence intensity measurements for FRAP experiments were carried out using densitometric analyses of the bleached cell areas/cells with the ImageJ Gels tool on an image stack. For this, a bleached cell and control cells in the same focus plane were cropped, and a montage of the time course was created separately. Densitometric analysis of the entire montage was carried out, thresholded equally over the entire time course using the straight line tool, and measured using the wand tool. Obtained fluorescence data were normalized to 100% before the bleach, and multiplied with a normalization factor obtained from the fluorescence values of the control cells to compensate for photobleaching effects.

Line scans of fluorescence micrographs were created in ImageJ using the Straight Line tool and Plot Profile command on individual channels of the processed respective RGB stack images.

Expanded View for this article is available online.

Author contributions

All authors (SS, SB, HDS) planned and performed experiments and carried out data analysis and interpretation. SS and HDS wrote the manuscript.

Conflict of interest

The authors declare that they have no conflict of interest.

References

Adams AE, Pringle JR (1991) Staining of actin with fluorochrome-conjugated phalloidin. *Methods Enzymol* 194: 729–731

Andag U, Neumann T, Schmitt HD (2001) The coatomer interacting protein Dsl1p is required for Golgi-to-ER retrieval in yeast. *J Biol Chem* 276: 39150–39160

Andag U, Schmitt HD (2003) Dsl1p, an essential component of the Golgi-endoplasmic reticulum retrieval system in yeast, uses the same sequence motif to interact with different subunits of the COPI vesicle coat. *J Biol Chem* 278: 51722–51734

Appenzeller-Herzog C, Hauri HP (2006) The ER-Golgi intermediate compartment (ERGIC): in search of its identity and function. *J Cell Sci* 119: 2173–2183

Arai S, Noda Y, Kainuma S, Wada I, Yoda K (2008) Ypt11 functions in bud-directed transport of the Golgi by linking Myo2 to the coatomer subunit Ret2. *Curr Biol* 18: 987–991

Bannykh SI, Rowe T, Balch WE (1996) The organization of endoplasmic reticulum export complexes. *J Cell Biol* 135: 19–35

Barlowe CK, Miller EA (2013) Secretory protein biogenesis and traffic in the early secretory pathway. *Genetics* 193: 383–410

Bevis BJ, Hammond AT, Reinke CA, Glick BS (2002) De novo formation of transitional ER sites and Golgi structures in Pichia pastoris. *Nat Cell Biol* 4: 750–756

Bharucha N, Liu Y, Papanikou E, McMahon C, Esaki M, Jeffrey PD, Hughson FM, Glick BS (2013) Sec16 influences transitional ER sites by regulating rather than organizing COPII. *Mol Biol Cell* 24: 3406–3419

Boehm J, Letourneur F, Ballensiefen W, Ossipov D, Demolliere C, Schmitt HD (1997) Sec12p requires Rer1p for sorting to coatomer (COPI)-coated vesicles and retrieval to the ER. *J Cell Sci* 110(Pt 8): 991–1003

Brennwald P, Kearns B, Champion K, Keranen S, Bankaitis V, Novick P (1994) Sec9 is a SNAP-25-like component of a yeast SNARE complex that may be the effector of Sec4 function in exocytosis. *Cell* 79: 245–258

Castillon GA, Watanabe R, Taylor M, Schwabe TM, Riezman H (2009) Concentration of GPI-anchored proteins upon ER exit in yeast. *Traffic (Copenhagen, Denmark)* 10: 186–200

Chua JJE (2014) Macromolecular complexes at active zones: integrated nano-machineries for neurotransmitter release. *Cell Mol Life Sci* 71: 3903–3916

Clay L, Caudron F, Denoth-Lippuner A, Boettcher B, Buvelot Frei S, Snapp EL, Barral Y (2014) A sphingolipid-dependent diffusion barrier confines ER stress to the yeast mother cell. *eLife* 3: e01883

Denoth Lippuner A, Julou T, Barral Y (2014) Budding yeast as a model organism to study the effects of age. *FEMS Microbiol Rev* 38: 300–325

Diefenbacher M, Thorsteinsdottir H, Spang A (2011) The Dsl1 tethering complex actively participates in soluble NSF (N-ethylmaleimide-sensitive factor) attachment protein receptor (SNARE) complex assembly at the endoplasmic reticulum in *Saccharomyces cerevisiae*. *J Biol Chem* 286: 25027–25038

Dodonova SO, Diestelkoetter-Bachert P, vonAppen A, Hagen WJ, Beck R, Beck M, Wieland F, Briggs JA (2015) VESICULAR TRANSPORT. A structure of the COPI coat and the role of coat proteins in membrane vesicle assembly. *Science (New York, NY)* 349: 195–198

Donovan KW, Bretscher A (2015) Tracking individual secretory vesicles during exocytosis reveals an ordered and regulated process. *J Cell Biol* 210: 181–189

van Drogen F, Stucke VM, Jorritsma G, Peter M (2001) MAP kinase dynamics in response to pheromones in budding yeast. *Nat Cell Biol* 3: 1051–1059

Estrada P, Kim J, Coleman J, Walker L, Dunn B, Takizawa P, Novick P, Ferro-Novick S (2003) Myo4p and She3p are required for cortical ER inheritance in *Saccharomyces cerevisiae*. *J Cell Biol* 163: 1255–1266

Farhan H, Weiss M, Tani K, Kaufman RJ, Hauri HP (2008) Adaptation of endoplasmic reticulum exit sites to acute and chronic increases in cargo load. *EMBO J* 27: 2043–2054

Farquhar MG, Palade GE (1981) The Golgi apparatus (complex)-(1954–1981)-from artifact to center stage. *J Cell Biol* 91: 77s–103s

Field C, Schekman R (1980) Localized secretion of acid phosphatase reflects the pattern of cell surface growth in *Saccharomyces cerevisiae*. *J Cell Biol* 86: 123–128

Finger FP, Hughes TE, Novick P (1998) Sec3p is a spatial landmark for polarized secretion in budding yeast. *Cell* 92: 559–571

Fredriksson S, Gullberg M, Jarvius J, Olsson C, Pietras K, Gustafsdottir SM, Ostman A, Landegren U (2002) Protein detection using proximity-dependent DNA ligation assays. *Nat Biotechnol* 20: 473–477

Ghaemmaghami S, Huh WK, Bower K, Howson RW, Belle A, Dephoure N, O'Shea EK, Weissman JS (2003) Global analysis of protein expression in yeast. *Nature* 425: 737–741

Ghosh I, Hamilton AD, Regan L (2000) Antiparallel leucine zipper-directed protein reassembly: application to the green fluorescent protein. *J Am Chem Soc* 122: 5658–5659

Gitler AD, Chesi A, Geddie ML, Strathearn KE, Hamamichi S, Hill KJ, Caldwell KA, Caldwell GA, Cooper AA, Rochet JC, Lindquist S (2009) Alpha-synuclein is part of a diverse and highly conserved interaction network that includes PARK9 and manganese toxicity. *Nat Genet* 41: 308–315

Glick BS (2014) Integrated self-organization of transitional ER and early Golgi compartments. *BioEssays* 36: 129–133

Govindan B, Bowser R, Novick P (1995) The role of Myo2, a yeast class V myosin, in vesicular transport. *J Cell Biol* 128: 1055–1068

Guo Y, Rebecchi M, Scarlata S (2005) Phospholipase Cbeta2 binds to and inhibits phospholipase Cdelta1. *J Biol Chem* 280: 1438–1447

He S, Ni D, Ma B, Lee JH, Zhang T, Ghozalli I, Pirooz SD, Zhao Z, Bharatham N, Li B, Oh S, Lee WH, Takahashi Y, Wang HG, Minassian A, Feng P, Deretic V, Pepperkok R, Tagaya M, Yoon HS *et al* (2013) PtdIns(3)P-bound UVRAG coordinates Golgi-ER retrograde and Atg9 transport by differential interactions with the ER tether and the beclin 1 complex. *Nat Cell Biol* 15: 1206–1219

Hirose H, Arasaki K, Dohmae N, Takio K, Hatsuzawa K, Nagahama M, Tani K, Yamamoto A, Tohyama M, Tagaya M (2004) Implication of ZW10 in membrane trafficking between the endoplasmic reticulum and Golgi. *EMBO J* 23: 1267–1278

Hu CD, Chinenov Y, Kerppola TK (2002) Visualization of interactions among bZIP and Rel family proteins in living cells using bimolecular fluorescence complementation. *Mol Cell* 9: 789–798

Huh WK, Falvo JV, Gerke LC, Carroll AS, Howson RW, Weissman JS, O'Shea EK (2003) Global analysis of protein localization in budding yeast. *Nature* 425: 686–691

Jahn R, Fasshauer D (2012) Molecular machines governing exocytosis of synaptic vesicles. *Nature* 490: 201–207

Jean S, Kiger AA (2012) Coordination between RAB GTPase and phosphoinositide regulation and functions. *Nat Rev Mol Cell Biol* 13: 463–470

Jose M, Tollis S, Nair D, Sibarita JB, McCusker D (2013) Robust polarity establishment occurs via an endocytosis-based cortical corralling mechanism. *J Cell Biol* 200: 407–418

Jose M, Tollis S, Nair D, Mitteau R, Velours C, Massoni-Laporte A, Royou A, Sibarita JB, McCusker D (2015) A quantitative imaging-based screen reveals the exocyst as a network hub connecting endo- and exocytosis. *Mol Biol Cell* 13: 2519–2534

Kaganovich D, Kopito R, Frydman J (2008) Misfolded proteins partition between two distinct quality control compartments. *Nature* 454: 1088–1095

Kamena F, Spang A (2004) Tip20p prohibits back-fusion of COPII vesicles with the endoplasmic reticulum. *Science (New York, NY)* 304: 286–289

Kamentsky L, Jones TR, Fraser A, Bray MA, Logan DJ, Madden KL, Ljosa V, Rueden C, Eliceiri KW, Carpenter AE (2011) Improved structure, function and compatibility for Cell Profiler: modular high-throughput image analysis software. *Bioinformatics* 27: 1179–1180

Kilmartin JV, Adams AE (1984) Structural rearrangements of tubulin and actin during the cell cycle of the yeast Saccharomyces. *J Cell Biol* 98: 922–933

Klumperman J (2011) Architecture of the mammalian Golgi. *Cold Spring Harb Perspect Biol* 3: a005181

Kodama Y, Hu CD (2010) An improved bimolecular fluorescence complementation assay with a high signal-to-noise ratio. *Biotechniques* 49: 793–805

Kohli M, Galati V, Boudier K, Roberson RW, Philippsen P (2008) Growth-speed-correlated localization of exocyst and polarisome components in growth zones of Ashbya gossypii hyphal tips. *J Cell Sci* 121: 3878–3889

Kraynack BA, Chan A, Rosenthal E, Essid M, Umansky B, Waters MG, Schmitt HD (2005) Dsl1p, Tip20p, and the novel Dsl3(Sec39) protein are required for the stability of the Q/t-SNARE complex at the endoplasmic reticulum in yeast. *Mol Biol Cell* 16: 3963–3977

Kurokawa K, Okamoto M, Nakano A (2014) Contact of cis-Golgi with ER exit sites executes cargo capture and delivery from the ER. *Nat Commun* 5: 3653

Ladinsky MS, Mastronarde DN, McIntosh JR, Howell KE, Staehelin LA (1999) Golgi structure in three dimensions: functional insights from the normal rat kidney cell. *J Cell Biol* 144: 1135–1149

Lerich A, Hillmer S, Langhans M, Scheuring D, van Bentum P, Robinson DG (2012) ER import Sites and Their Relationship to ER Exit Sites: A New Model for Bidirectional ER-Golgi Transport in Higher Plants. *Front Plant Sci* 3: 143

Levi SK, Bhattacharyya D, Strack RL, Austin JR 2nd, Glick BS (2010) The yeast GRASP Grh1 colocalizes with COPII and is dispensable for organizing the secretory pathway. *Traffic (Copenhagen, Denmark)* 11: 1168–1179

Li R, Gundersen GG (2008) Beyond polymer polarity: how the cytoskeleton builds a polarized cell. *Nat Rev Mol Cell Biol* 9: 860–873

Lipatova Z, Belogortseva N, Zhang XQ, Kim J, Taussig D, Segev N (2012) Regulation of selective autophagy onset by a Ypt/Rab GTPase module. *Proc Natl Acad Sci USA* 109: 6981–6986

Lipatova Z, Kim J, Segev N (2015) Ypt1 and TRAPP Interactions: optimization of Multicolor Bimolecular Fluorescence Complementation in Yeast. In *Rab GTPases*, Li G (ed), pp 107–116. New York: Springer

Liu B, Larsson L, Caballero A, Hao X, Öling D, Grantham J, Nyström T (2010) The polarisome is required for segregation and retrograde transport of protein aggregates. *Cell* 140: 257–267

Magliery TJ, Regan L (2005) Sequence variation in ligand binding sites in proteins. *BMC Bioinformatics* 6: 240

Magliery TJ, Wilson CG, Pan W, Mishler D, Ghosh I, Hamilton AD, Regan L (2005) Detecting protein-protein interactions with a green fluorescent protein fragment reassembly trap: scope and mechanism. *J Am Chem Soc* 127: 146–157

Mao K, Wang K, Liu X, Klionsky DJ (2013) The scaffold protein Atg11 recruits fission machinery to drive selective mitochondria degradation by autophagy. *Dev Cell* 26: 9–18

Mardones GA, Snyder CM, Howell KE (2006) Cis-Golgi matrix proteins move directly to endoplasmic reticulum exit sites by association with tubules. *Mol Biol Cell* 17: 525–538

McCusker D, Royou A, Velours C, Kellogg D (2012) Cdk1-dependent control of membrane-trafficking dynamics. *Mol Biol Cell* 23: 3336–3347

Meiringer CT, Rethmeier R, Auffarth K, Wilson J, Perz A, Barlowe C, Schmitt HD, Ungermann C (2011) The Dsl1 protein tethering complex is a resident endoplasmic reticulum complex, which interacts with five soluble NSF (N-ethylmaleimide-sensitive factor) attachment protein receptors (SNAREs): implications for fusion and fusion regulation. *J Biol Chem* 286: 25039–25046

Miaczynska M, Zerial M (2002) Mosaic organization of the endocytic pathway. *Exp Cell Res* 272: 8–14

Morell M, Espargaro A, Aviles FX, Ventura S (2007) Detection of transient protein-protein interactions by bimolecular fluorescence complementation: the Abl-SH3 case. *Proteomics* 7: 1023–1036

Nagai T, Ibata K, Park ES, Kubota M, Mikoshiba K, Miyawaki A (2002) A variant of yellow fluorescent protein with fast and efficient maturation for cell-biological applications. *Nat Biotechnol* 20: 87–90

Nelson JC, Stavoe AK, Colon-Ramos DA (2013) The actin cytoskeleton in presynaptic assembly. *Cell Adh Migr* 7: 379–387

Okamoto M, Kurokawa K, Matsuura-Tokita K, Saito C, Hirata R, Nakano A (2012) High-curvature domains of the ER are important for the organization of ER exit sites in Saccharomyces cerevisiae. *J Cell Sci* 125: 3412–3420

Pelham HRB (1996) The dynamic organisation of the secretory pathway. *Cell Struct Funct* 21: 413–419

Pruyne DW, Schott DH, Bretscher A (1998) Tropomyosin-containing actin cables direct the Myo2p-dependent polarized delivery of secretory vesicles in budding yeast. *J Cell Biol* 143: 1931–1945

Rappoport JZ, Simon SM (2003) Real-time analysis of clathrin-mediated endocytosis during cell migration. *J Cell Sci* 116: 847–855

Reinke CA, Kozik P, Glick BS (2004) Golgi inheritance in small buds of Saccharomyces cerevisiae is linked to endoplasmic reticulum inheritance. *Proc Natl Acad Sci USA* 101: 18018–18023

Ren Y, Yip CK, Tripath IA, Huie D, Jeffrey PD, Walz T, Hughson FM (2009) A structure-based mechanism for vesicle capture by the multisubunit tethering complex Dsl1. *Cell* 139: 1119–1129

Ronchi P, Tischer C, Acehan D, Pepperkok R (2014) Positive feedback between golgi membranes, microtubules and ER-exit sites directs golgi de novo biogenesis. *J Cell Sci* 127: 4620–4633

Rossanese OW, Soderholm J, Bevis BJ, Sears IB, O'Connor J, Williamson EK, Glick BS (1999) Golgi structure correlates with transitional endoplasmic reticulum organization in Pichia pastoris and Saccharomyces cerevisiae. *J Cell Biol* 145: 69–81

Rossanese OW, Reinke CA, Bevis BJ, Hammond AT, Sears IB, O'Connor J, Glick BS (2001) A role for actin, Cdc1p, and Myo2p in the inheritance of late Golgi elements in Saccharomyces cerevisiae. *J Cell Biol* 153: 47–62

Rutz C, Satoh A, Ronchi P, Brugger B, Warren G, Wieland FT (2009) Following the fate in vivo of COPI vesicles generated in vitro. *Traffic (Copenhagen, Denmark)* 10: 994–1005

Sato K, Sato M, Nakano A (2001) Rer1p, a retrieval receptor for endoplasmic reticulum membrane proteins, is dynamically localized to the Golgi apparatus by coatomer. *J Cell Biol* 152: 935–944

Sato K, Sato M, Nakano A (2003) Rer1p, a retrieval receptor for ER membrane proteins, recognizes transmembrane domains in multiple modes. *Mol Biol Cell* 14: 3605–3616

Schmid M, Jaedicke A, Du TG, Jansen RP (2006) Coordination of endoplasmic reticulum and mRNA localization to the yeast bud. *Curr Biol* 16: 1538–1543

Schmidt C, Peng B, Li Z, Sclabas GM, Fujioka S, Niu J, Schmidt-Supprian M, Evans DB, Abbruzzese JL, Chiao PJ (2003) Mechanisms of proinflammatory cytokine-induced biphasic NF-kappaB activation. *Mol Cell* 12: 1287–1300

Schmitt HD (2010) Dsl1p/Zw10: common mechanisms behind tethering vesicles and microtubules. *Trends Cell Biol* 20: 257–268

Schott D, Ho J, Pruyne D, Bretscher A (1999) The COOH-terminal domain of Myo2p, a yeast myosin V, has a direct role in secretory vesicle targeting. *J Cell Biol* 147: 791–808

Schott DH, Collins RN, Bretscher A (2002) Secretory vesicle transport velocity in living cells depends on the myosin-V lever arm length. *J Cell Biol* 156: 35–39

Schröder-Köhne S, Letourneur F, Riezman H (1998) Alpha-COP can discriminate between distinct, functional di-lysine signals in vitro and regulates access into retrograde transport. *J Cell Sci* 111(Pt 23): 3459–3470

Shaywitz DA, Espenshade PJ, Gimeno RE, Kaiser CA (1997) COPII subunit interactions in the assembly of the vesicle coat. *J Biol Chem* 272: 25413–25416

Shcheprova Z, Baldi S, Frei SB, Gonnet G, Barral Y (2008) A mechanism for asymmetric segregation of age during yeast budding. *Nature* 454: 728–734

Sheu Y-J, Santos B, Fortin N, Costigan C, Snyder M (1998) Spa2p interacts with cell polarity proteins and signaling components involved in yeast cell morphogenesis. *Mol Cell Biol* 18: 4053–4069

Shindiapina P, Barlowe C (2010) Requirements for transitional endoplasmic reticulum site structure and function in *Saccharomyces cerevisiae. Mol Biol Cell* 21: 1530–1545

daSilva LL, Snapp EL, Denecke J, Lippincott-Schwartz J, Hawes C, Brandizzi F (2004) Endoplasmic reticulum export sites and Golgi bodies behave as single mobile secretory units in plant cells. *Plant Cell* 16: 1753–1771

Spang A (2009) On vesicle formation and tethering in the ER-Golgi shuttle. *Curr Opin Cell Biol* 21: 531–536

Spang A (2012) The DSL1 complex: the smallest but not the least CATCHR. *Traffic (Copenhagen, Denmark)* 13: 908–913

Strack RL, Hein B, Bhattacharyya D, Hell SW, Keenan RJ, Glick BS (2009) A rapidly maturing far-red derivative of DsRed-Express2 for whole-cell labeling. *Biochemistry* 48: 8279–8281

Suckling RJ, Poon PP, Travis SM, Majoul IV, Hughson FM, Evans PR, Duden R, Owen DJ (2015) Structural basis for the binding of tryptophan-based motifs by delta-COP. *Proc Natl Acad Sci USA* 112: 14242–14247

Sung MK, Huh WK (2007) Bimolecular fluorescence complementation analysis system for in vivo detection of protein-protein interaction in *Saccharomyces cerevisiae. Yeast (Chichester, England)* 24: 767–775

Thumm M, Egner R, Koch B, Schlumpberger M, Straub M, Veenhuis M, Wolf DH (1994) Isolation of autophagocytosis mutants of *Saccharomyces cerevisiae. FEBS Lett* 349: 275–280

Tokuyasu KT (1980) Immunochemistry on ultrathin frozen sections. *Histochem J* 12: 381–403

Tripathi A, Ren Y, Jeffrey PD, Hughson FM (2009) Structural characterization of Tip20p and Dsl1p, subunits of the Dsl1p vesicle tethering complex. *Nat Struct Mol Biol* 16: 114–123

Walch-Solimena C, Collins RN, Novick PJ (1997) Sec2p mediates nucleotide exchange on Sec4p and is involved in polarized delivery of post-Golgi vesicles. *J Cell Biol* 137: 1495–1509

Wang M, Herrmann CJ, Simonovic M, Szklarczyk D, von Mering C (2015) Version 4.0 of PaxDb: protein abundance data, integrated across model organisms, tissues, and cell-lines. *Proteomics* 15: 3163–3168

Watson LJ, Rossi G, Brennwald P (2014) Quantitative analysis of membrane trafficking in regulation of Cdc42 polarity. *Traffic (Copenhagen, Denmark)* 15: 1330–1343

Weber-Boyvat M, Zhao H, Aro N, Yuan Q, Chernov K, Peranen J, Lappalainen P, Jantti J (2013) A conserved regulatory mode in exocytic membrane fusion revealed by Mso1p membrane interactions. *Mol Biol Cell* 24: 331–341

Whaley WG, Dauwalder M, Leffingwell TP (1975) Differentiation of the Golgi apparatus in the genetic control of development. *Curr Top Dev Biol* 10: 161–186

Yu IM, Hughson FM (2010) Tethering factors as organizers of intracellular vesicular traffic. *Annu Rev Cell Dev Biol* 26: 137–156

Zacharias DA, Violin JD, Newton AC, Tsien RY (2002) Partitioning of lipid-modified monomeric GFPs into membrane microdomains of live cells. *Science (New York, NY)* 296: 913–916

Zink S, Wenzel D, Wurm CA, Schmitt HD (2009) A link between ER tethering and COP-I vesicle uncoating. *Dev Cell* 17: 403–416